THE UNIVERSITY OF MANITOBA

ELECTROLUMINESCENCE IN ANTHRACENE CRYSTALS UNDER TIME VARYING ELECTRIC FIELDS

by

HENRY PETER KUNKEL

A THESIS

SUBMITTED TO THE FACULTY OF GRADUATE STUDIES

IN PARTIAL FULFILLMENT OF THE REQUIREMENTS FOR THE DEGREE

OF MASTER OF SCIENCE

DEPARTMENT OF ELECTRICAL ENGINEERING

WINNIPEG, MANITOBA

APRIL, 1975

ELECTROLUMINESCENCE IN ANTHRACENE CRYSTALS UNDER TIME VARYING ELECTRIC FIELDS

by

HENRY PETER KUNKEL

A dissertation submitted to the Faculty of Graduate Studies of the University of Manitoba in partial fulfillment of the requirements of the degree of

MASTER OF SCIENCE

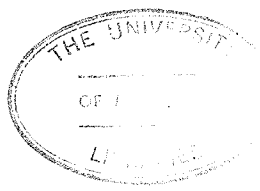

ABSTRACT

Electroluminescence in anthracene single crystals has been systematically studied, using a sodium electrode as the electron-injecting contact and a silver electrode as the hole-injecting contact, under time varying electric fields at various temperatures. The results show that the electroluminescent brightness decreases monotonically with increasing frequency for the frequency range from 20 Hz to 10 KHz and over the temperature range from -20°C to 40°C. At 10 KHz the electroluminescent brightness is almost undetectable and one-half the period of this frequency has been taken as the time required for the injected carriers to meet each other to produce electroluminescence. In general the brightness increases with increasing temperature, reaches a peak at a critical temperature, and then decreases with increasing temperature. This critical temperature is about 20°C for a.c. fields and about 40°C for half-wave rectified a.c. fields, and this phenomenon is attributed to a smaller space charge created by the a.c. than by the d.c. fields. There is a delay time between the application of the fields and the appearance of electroluminescence, and this delay time decreases with increasing frequency and saturates at a value which is associated with the transit time of the electrons across the sample. The large delay time at low frequencies is associated with the time taken for an electron space charge to build up near the anode to enhance hole injection from the anode.

ACKNOWLEDGEMENTS

The author wishes to express his sincere appreciation to Dr. K.C. Kao for suggesting this thesis subject and for his supervision of the project.

The author also wishes to extend his sincere thanks to Dr. W. Hwang for his valuable assistance and many discussions.

Sincere thanks are given to the graduate students of the Materials Research Laboratory and the staff of the Electrical Engineering Department of the University of Manitoba for their assistance and co-operation.

Henry P. Kunkel

TABLE OF CONTENTS

LIST OF FIGURES

CHAPTER I

INTRODUCTION

Electroluminescence is produced in the bulk of a crystal by the recombination of electrons and holes injected into the crystal from injecting electrodes. In organic semiconductors the recombination of electrons and holes leads to the formation of triplet and singlet excitons. It is the radiative decay of singlet excitons which produces electroluminescence. Anthracene has become a model material upon which a great deal of the work in organic semiconductors has been done. Electroluminescence in anthracene using a pair of double injecting electrodes has been observed by many investigators [14, 18, 30]. A great deal of study has gone into the properties of d.c. electroluminescence. Very little work, however, has been done on the properties of electroluminescence resulting from time varying voltages. It is the purpose of this investigation to determine the frequency and temperature dependence of the electroluminescence. Also, the phase relationship between the electroluminescence and the applied voltage will be investigated.

In Chapters II, III, and IV a review will be presented on the properties of the excitons in anthracene, the processes involved in electroluminescences and the properties of d.c. electroluminescence. Chapter V will describe the experimental procedures involved in this investigation and Chapter VI will present and discuss the results obtained. The conclusions will be given in Chapter VII.

CHAPTER II

EXCITONS IN ANTHRACENE

The study of excitons in anthrancene crystals began in 1963 with the discovery that red light from a ruby laser cangenerate detectable concentrations of triplet excitons (mobile neutral electronic excited state of a crystal with spin of 1) in spite of the low probability for this transition [20]. Experimental and theoretical studies of the exciton have subsequently become an active area of research in the field of organic semiconductors. Anthracene has become a model system for these materials upon which a great deal of research has been conducted.

In organic crystals, such as anthracene, weak Van der Waals attractions bind the molecules together. The intermolecular interactions can thus be regarded as a weak perturbation to a non-interacting array of molecules. The electronic energy levels in the crystal are in fact indentifiable with the molecular states. Figure (2.1) shows the electronic energy levels, for the isolated anthracene molecule, from which the exciton bands arise.

In studying the dynamic properties of excitons we need only to consider the lowest singlet and triplet exciton bands since any higher exciton state which is populated, rapidly undergoes a radiationless decay to the lowest state.

A most interesting property of triplet exictons is the mutual annihilation of pairs of triplets resulting in the production of a singlet. The lifetime of singlet excitons in anthracene has been reported to be approximately 10^{-8} sec [39, 48]. The characteristic blue flourescence resulting from the decay of directly generated singlets is thus called

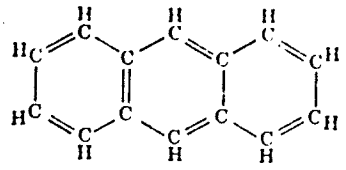

anthracene molecule

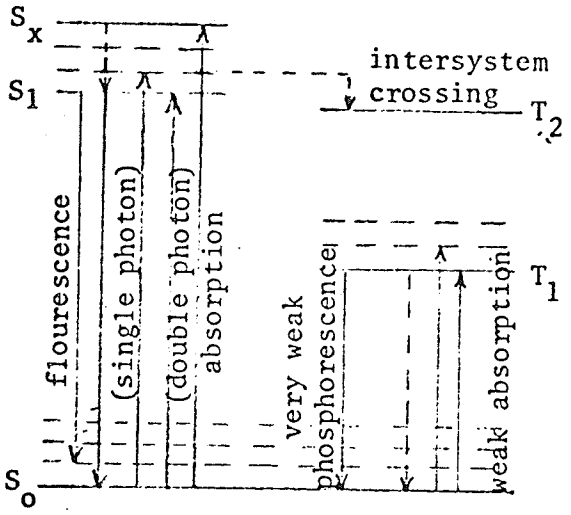

Fig. 2.1 Electronic energy level for anthracene molecule

Excitons in molecular crystals are best described by the Frenkel or tight-binding model of the exciton. A Frenkel exciton is essentially an excited state of a single atom (molecule), but the excitation can hop from one atom (molecule) to another because of the coupling between neighbouring atoms (molecules). The figure shows the electronic energy levels for the isolated anthracene molecule from which the exciton bands arise. The singlet and triplet manifolds are split to sublevels due to molecular vibrations (dashed horizontal lines). The solid lines represent radiative transitions and the dashed non-radiative transitions. In the crystal the S_o-S_1 energy difference and the S_o-T_1 energy difference are 3.42 eV and 1.80 eV respectively.

prompt flourescence. The lifetime of the triplet exciton varies from less than a millisecond to 25 m sec depending on the purity of the sample [39, 48]. Thus flourescence resulting from singlets produced by the annihilation of pairs of triplets is delayed by six orders of magnitude longer than the prompt flourescence. This component is called "delayed flourescence". Thus the irradiation of anthracene crystals by light corresponding to the triplet absorption region (14,720 cm^{-1}) gives rise to delayed flourescence (25,000 cm^{-1}). The triplet exciton concentration is governed by the equation [35]

$$\frac{d[T]}{dt} = G_T - \beta[T] - \gamma[T]^2 \qquad (2.1)$$

where G_T is the exciton generation rate (which for optical experiments is given by αI where α and I are, respectively, the absorption coefficient and illumination intensity) β is the unimolecular triplet decay constant and γ is the triplet-triplet annihilation rate constant. The singlet exciton concentration $[S]$ is governed by the equation [35]

$$\frac{d[S]}{dt} = -\alpha [S] + \frac{1}{2}\gamma[S]^2 \qquad (2.2)$$

where α is the flourescence rate constant. For low exciton concentrations, $\gamma[T]^2 << \beta[T]$ and under steady state conditions, $\frac{d[S]}{dt} = \frac{d[T]}{dt} = 0$, the intensity of the delayed florescence is

$$I_F = \alpha[S] = \frac{1}{2}\gamma \left(\frac{G_T}{\beta}\right)^2 \qquad (2.3)$$

The intensity of the delayed flourescence is proportional to the square of the triplet exciton generation rate, provided that the triplet concentration is sufficiently low to ensure that the majority of the triplets decay to the ground state by a radiationless monomolecular process. At higher

triplet concentrations, however, bimolecular decay predominates and the delayed flourescence intensity becomes directly proportional to the triplet generation rate.

The flourescence intensity is temperature dependent through the temperature dependence of flourescence reabsorption which, for anthracene, is approximated by the linear relationship [35]

$$R = 10^{7} \ (1 - 7 \times 10^{-3} T) \tag{2.4}$$

Since β and γ have been shown to be essentially temperature independent by Singh et al. [36], the delayed flourescence should vary with temperature according to equation (2.4). Singh and Lipsett [37], however, have reported that the intensity of flourescence due to triplet-triplet annihilations exhibits an anamolous temperature dependence involving several distinct maxima (Figure 2.2).

To interpret this phenomena Siebrand [35] has developed a kinetic model based on the trapping of triplet excitons. At low temperatures the excitons may become trapped and much of the florescence is due to the annihilation of trapped excitons by free excitons. In general, this would tend to reduce the bimolecular annihilation and also the flourescence intensity. However, if the trapped triplet excitons have a long lifetime as compared to the free excitons then the reverse may occur due to the fact that the annihilation rate is proportional to the square of the triplet lifetime. We denote the concentration of traps of type i and depth ε_i by N_i, the concentration of traps occupied by triplet excitons by $[T_i]$ and the lifetime of the trapped triplets by β_i^{-1}. The trapping and release rates associated with trap i are given respectively by

$$b_i = Z_i \ (N_i - [T_i]) = P_i - Z_i [T_i]$$

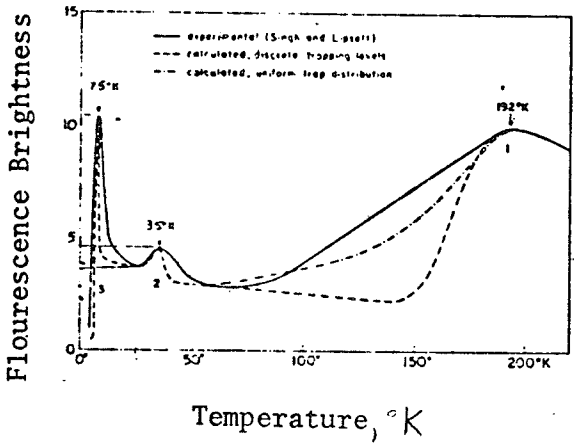

Fig. 2.2 Delayed flourescence as a function of temperature for undoped anthracene crystal. (After Siebrand [34].)

$$q_i = Z_i \, N \exp(-\varepsilon_i/KT)$$

where Z_i is the collision rate between free excitons and traps of type i, which depends on the transport properties of the triplet exciton, and N is the number of molecules per unit volume. Equations (2.1) to (2.3) with trapping become

$$\frac{d[T]}{dt} = \alpha I + \sum_i q_i [T_i] - (\beta + \sum_i P_i - \sum_i Z_i [T_i] + \Sigma \gamma_i [T_i]) \, [T] - \gamma [T]^2 = 0 \qquad (2.5)$$

$$\frac{d[T_i]}{dt} = \alpha_i I + P_i [T] - (q_i + \beta_i + Z_i \, [T] + \gamma_i [T]) \, [T_i] = 0 \qquad (2.6)$$

$$\frac{d[S]}{dt} = - \alpha [S] + \frac{1}{2} \gamma [T]^2 + \frac{1}{2} [T] \sum_i \gamma_i \, [T_i] \qquad (2.7)$$

where γ_i is the annihilation rate constant of free and trapped excitons. These equations have been solved by Siebrand [35], for low levels of excitation, with the assumptions that

(1) direct absorption by the traps, that is direct trapped exciton generation, is not important ($\alpha_i = 0$),

(2) the traps are not saturated ($Z_i \, [T] \, [T_i] = 0$),

(3) all bimolecular triplet terms are negligible compared to the unimolecular term, that is, a negligible fraction of the free or trapped triplet excitons decay by triplet-triplet annihilations ($\gamma [T]^2$ and $\gamma_i \, [T] \, [T_i]$ are small), and

(4) The collision cross-section of all trapped triplet excitons are equal.

With the above assumptions equation (2.3) becomes

$$I_F = \frac{1}{2} \gamma \left(\frac{\alpha I}{\beta}\right) B \qquad (2.8)$$

where

$$B = \frac{(1 + \sum_i A_i)}{(1 + \sum_i \rho_i A_i)^2} \tag{2.9}$$

$$A_i = \frac{P_i}{(\beta_i + q_i)} \tag{2.10}$$

$$\rho_i = \frac{\beta_i}{\beta} \tag{2.11}$$

Extrema in the $I_F(T)$ curve occur whenever

$$\frac{dB}{dt} = 0 \qquad \text{or}$$

$$\sum_i A_i' \left[1 + \sum_i \rho_i A_j - 2\rho_i \left(1 + \sum_i A_j\right)\right] = 0 \tag{2.12}$$

where $A_i' = \frac{dA_i}{dT}$. A_i' goes to zero in two limiting situations: at relatively high temperatures where $q_i >> P_i$ and the traps are ineffective and at relatively low temperatures where $q_i << \beta_i$ and the trapped exciton decays before it can escape. If the traps are a set of energetically well separated discrete levels we can expect temperature regions where all A_i' are zero to alternate with regions where all but one A_i' are zero. For a range of finite A_i' equation (2.12) demands that

$$1 + \sum_i \rho_j A_j - 2 \rho_i \left(1 + \sum_j A_j\right) = 0$$

or

$$\rho_i = \frac{(1 + \sum_j{}' \rho_j A_j)}{2 + A_i + 2\sum_i A_j'} \tag{2.13}$$

where the prime on the summation indicates the term $j=i$ is omitted. Combining equations (2.13) and (2.9) we have

$$B^{i}_{ext} = [4\rho_i^{\,2} (1 + \sum_{j}{}' A_j)]^{-1} \tag{2.14}$$

All traps with $j > i$ are empty so that $A_{j>i} \simeq 0$. All traps with $j<i$ are filled and therefore $A_{j<i} \simeq \rho_j/\beta_j$. For the special case where only one trapping level is operative equations (2.13) and (2.14) reduce to

$$\rho_1 = (2 + A_1)^{-1} \tag{2.15}$$

$$B_{extr} = [4\rho_1 (1 - \rho_1)]^{-1} = \beta^2/4\beta_1 (\beta - \beta_1) \tag{2.16}$$

Since $A_1 > 0$ we can conclude from equation (2.15) that $\beta_1 < \frac{1}{2}\beta$. It follows that for the case of a single trapping level B has a maximum if the lifetime of the trapped triplet exciton is more than twice the lifetime of the free exciton. Similar arguments apply to the more general case described by equations (2.13) and (2.14). The two limiting conditions for $A_i' = 0$ result in two minima whenever equation (2.14) gives rise to a maximum. From equation (2.14) it is also seen that the relative heights of the maxima should be an increasing function of temperature unless the triplet lifetime is longer for the shallower traps. This is because of the monotonic decrease of ΣA_j with temperature.

Siebrand's analysis completely describes every discrete trap with three parameters ϵ_i, N_i and β_i which can be obtained from the $I_F[T]$ curve by means of equations (2.12) to (2.14). With the proper choice of parameters Siebrand [35] has been able to approximately reproduce the experimental results of Singh and Lipsett using a three discrete trap model (the solid curve of Figure 2.2). Siebrand has obtained a better agreement by assuming a diffuse trap distribution for the high temperature

trap. This result is shown in the dot-dash line in Figure 2.2. The discrepancy that remains could indicate that there are more than three discrete (distributed) traps.

In his theory Siebrand assumed that all triplet-triplet annihilations contributed to the formation of flourescing singlet states. If all triplet spin states occur with equal probability, however, no more than one collision in nine can lead to a singlet. Goode and Lipsett [11] have therefore replaced that total annihilation rates γ and γ_i by radiative annihilation rates $f\gamma$ and $f'\gamma_i$, where $f\gamma$ is the component of the free triplet annihilation rate γ and $f'\gamma_i$ is the component of the free-trapped annihilation rate γ_i that lead to the formation of florescing states. Since the collision rate restricts the magnitude of the annihilation rate, we have that $Z_i > \gamma_i \geq f'\gamma_i$ where $Z_i \geq qf'\gamma_i$.

Goode and Lipsett [11] have studied the relationship between delayed florescence and excitation intensity at low temperature and have found deviations from the square law at comparatively low excitation intensities. To account for the deviations from the square law Goode and Lipsett have extended the theory of Siebrand to include the saturation of triplet traps (the term $Z_i[T][T_i]$) as well as the depopulation of free and trapped triplets by bimolecular annihilation (the terms $\gamma_i[T][T_i]$ and $\gamma[T]^2$). The expression obtained gives a reasonable agreement with the experimental results.

At room temperature the triplet traps are not effective and the square law deviation is due to free exciton annihilation only. Thus, for small exciton concentrations the deviation is negligible as expected.

Figure 2.3 gives a detailed description of the exciton transitions possible in organic crystals. The solid lines represent radiative transitions and the dashed lines represent non-radiative transitions. It is assumed that the singlet and triplet excitons have generation rates of G_S and G_T respectively. The singlet and triplet excitons have the rate constants α_1 and β_1, respectively, for the radiative transitions to the ground state with the emission of photons. The rate constants for the non-radiative transitions with the emission of phonons is given by α_2 and β_2. Singlet and triplet excitons may relax into traps at a level ϵ_t lower in energy with the rate constants α_i and β_i respectively. Trapped excitons may be thermally detrapped and then decay radiatively with the rate constant α_{i1} and β_{i1} and non-radiatively with the rate constants α_{i2} and β_{i2} for the singlet and triplet excitons, respectively. The effective rate constant for triplet-triplet annihilation is given by γ and that for triplet-trapped triplet annihilation is given by γ_i. The rate constant for the production of singlet excitons from the triplet-triplet annihilation (triplet-triplet annihilation may lead to a higher energy triplet) is given by $f\gamma$ and from triplet-trapped triplet annihilation by $f'\gamma_i$. The singlet exciton (S) may also make a transition to the triplet state (T_1) via a higher energy triplet state (T_2). This is referred to as intersystem crossing. Adolf et al. [1] have shown that this process is neglegible compared to the radiative decay of singlet excitons. Siebrand et al., in their analysis of the temperature dependence of the delayed flourescence in anthracene, have also assumed that the non-radiative decay mechanism of singlet and triplet excitons, as well as the prescence of singlet traps, can be ignored.

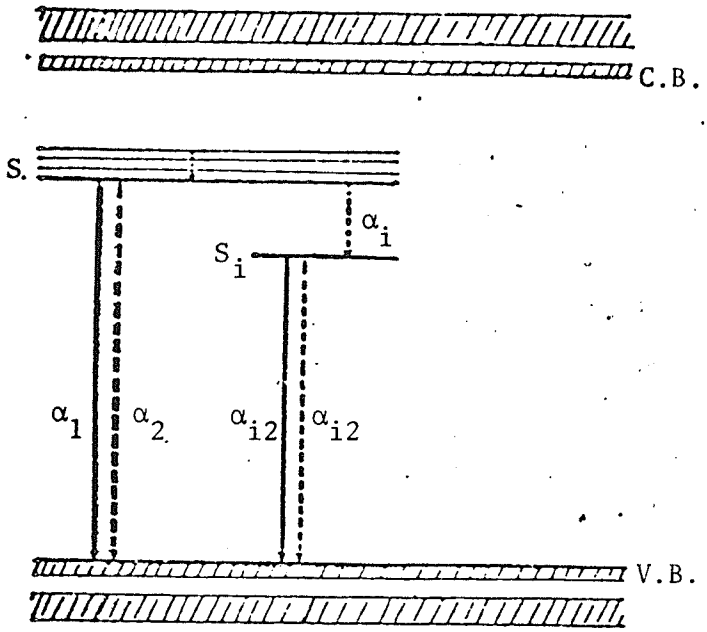

(a)

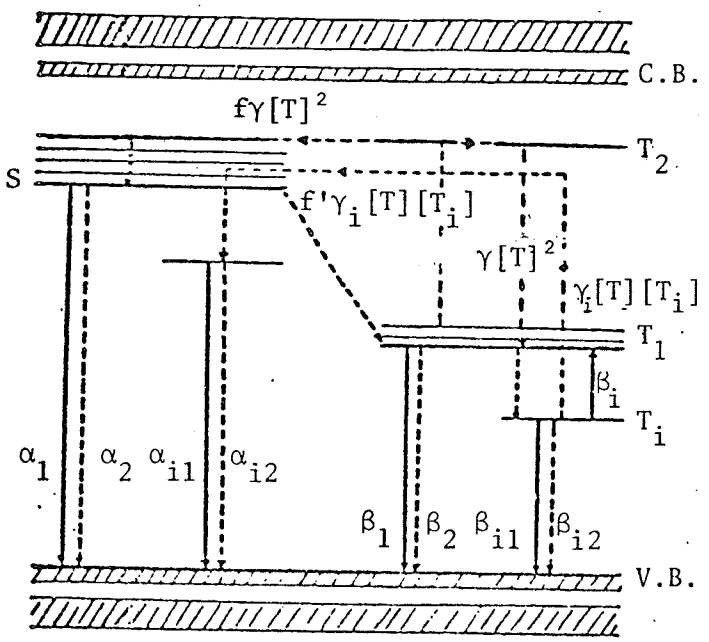

(b)

Fig. 2.3 Exciton transitions in organic crystals. Solid lines, radiative transition; dashed lines, non-radiative transition.
(a) prompt flourescence
(b) delayed flourescence

CHAPTER III

ELECTROLUMINESCENCE

Electroluminescence is produced in the bulk of a crystal by direct recombination of electrons and holes injected into the crystal from injecting electrodes. Electron-hole recombination may lead to both radiative and non-radiative transitions. It is generally accepted [14] that the recombination of injected holes and electrons in organic semiconductors will yield singlet and triplet excitons and the electroluminescence is produced by the radiative decay of the singlet excitons. The quantum yield of electroluminescence will depend on the probability of radiative and non-radiative transitions and on the efficiency of producing the radiative exciton. In this chapter we will discuss the mechanisms of electroluminescence and also the dominant non-radiative transitions of the exciton.

3.1 Electron-hole Recombination

Electron-hole recombination involves two steps. First the electron and hole must come close enough to one another to be trapped by the other's coulomb field. This can occur in a radius around the carriers given by [16]

$$r_{kT} = \frac{2e^2}{3\epsilon kT} \tag{3.1}$$

A carrier within this sphere must loose sufficient energy through scattering to become trapped. For this to occur the mean free path of the carrier must be small compared to the radius r_{kT} the Coulomb capture radius. For anthracene $\epsilon = 3.14\ \epsilon_o$ and $r_{kT} = 120\ \text{Å}$ at room temperature. The mean free path of the carriers in anthracene is only

a few lattice parameters [14, 26]. Thus the rate determining process for electron-hole recombination is the diffusion of oppositely charged particles toward each other. This satisfies the conditions for which Langevin's theory of carrier recombination applies [26]. The relative drift velocity of a positive and negative charge when they are a distance r apart is

$$V_d = (\mu_+ + \mu_-) \frac{q}{\varepsilon r^2} \tag{3.2}$$

where μ_+ and μ_- are the drift mobilities of the positive and negative charges respectively. The recombination rate will be the flow rate of positive charges into a sphere of radius r around a negative charge. Thus, the recombination rate is

$$K = 4\pi r^2 \varepsilon V_d = 4\pi q (\mu_+ + \mu_-) \tag{3.3}$$

If we take $\mu_+ + \mu_- \simeq 2\ cm^2\ V^{-1}\ sec^{-1}$ the recombination rate will be $1.2 \times 10^{-6}\ cm^2\ V^{-1}\ sec^{-1}$. This compares very well with experimentally determined values [38].

The recombination of electrons and holes in organic semiconductors will yield singlet and triplet excitons. It is generally assumed that

(1) the rates of production of singlet and triplet excitons is proportional to the multiplicities of the state, that is three times as many triplets as singlets are generated, and

(2) the annihilation of a pair of triplets can produce either an electronically or vibronically excited triplet exciton or a singlet exciton. Since three times as many pairs of excitons have total spin one than have a total spin of zero, this suggests that triplet-triplet annihilations will produce three times more triplets than singlet excitons. The kinetics of the above model can be described by

$$4(e+h) \rightarrow 1S + 3T \tag{3.4}$$

$$8T \rightarrow 1S + 3T^{*} \tag{3.5}$$

Since any excited triplet state decays back to the lowest triplet state in a time much shorter than the lifetime of the latter, reaction (3.5) becomes

$$5T \rightarrow 1S \tag{3.6}$$

Combining equations (3.4) and (3.6) gives

$$20(e+h) \rightarrow 5\ S_{dir} + 15T \rightarrow 5\ S_{dir} + 3\ S_{ind} \tag{3.7}$$

where e and h represent the electron and hole and S and T the singlet and triplet excitons respectively.

3.2 Exciton-Carrier Interactions

Quenching of delayed flourescence by injected carriers is observed when either monomoledulor or bimoleculor exciton processes are the dominant exciton-decay mechanism. With small triplet exciton densities, injected carriers reduce the triplet lifetime and hence the delayed floure-scence intensity [42, 43, 13]. Figure 3.1 shows the variation of the triplet exciton lifetime with injected free carrier densities as obtained by Wakayama and Williams [43]. If the carriers are not trapped then the triplet lifetime τ will obey the relation

$$\frac{1}{\tau} - \frac{1}{\tau_o} = kn \tag{3.8}$$

where $n = \frac{3}{2}\ \varepsilon\varepsilon_o\ \frac{V}{eL^2}$ is the carrier density, τ_o is the triplet lifetime in the absence of any injected carriers and k is the exciton-carrier interaction rate constant. When the triplet density is large, however,

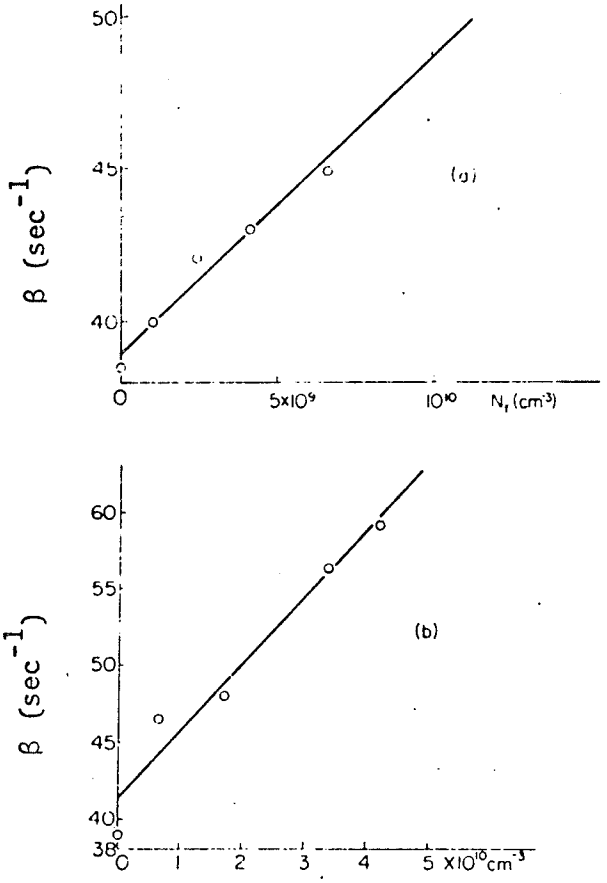

Fig. 3.1 The triplet exciton lifetime as a function of injected free carrier density for (a) holes and (b) electrons at room temperature. (After Wakayama and Wilfliams [43].)

this reduction in triplet lifetime becomes ineffective. The delayed flourescence intensity does, however, decrease in the presence of injected carriers. Wakayama and Williams [43] have shown that the interaction of charge carriers with the singlet exciton produced by triplet-triplet annihilation cannot satisfactorily explain this drop in flourescence intensity. Thus in the case of high triplet concentrations the most significant effect of the presence of charge carriers is not on either the triplet or singlet exciton, but rather on some intermediate state.

The formation of a triplet pair state during the triplet annihilation process has been suggested by several studies [40]. Wakayama and Williams have developed the following kinetic model which uses this pair state to account for the flourescence quenching. K(N) represents the interaction rate constant between the carriers and the pair states.

$$T + T \underset{K_{-1}}{\overset{K_1}{\leftrightarrow}} |TT\rangle \begin{cases} \xrightarrow{K_{2S}} S \xrightarrow{K_3} S_o \\ \xrightarrow{K_{2T}} T \\ \xrightarrow{K(N)} 2S_o \end{cases} \qquad (3.9)$$

The triplet pair state $|TT\rangle$ consists of two triplet excitons which are close enough to interact. K(N) can be expressed in terms of the interaction cross section, σ, between the carrier and the intermediate state, their thermal velocities u and ν respectively and the ratio of free to total carrier density, θ. [43]

$$\begin{aligned} K(N) &= \nu N_t (1 - \theta)\sigma + \theta N_t \sigma (u + \frac{\nu^2}{3u}) \qquad u > \nu \\ &= \nu N_t (1 - \theta)\sigma + \theta N_t \sigma (\nu + \frac{u^2}{3\nu}) \qquad u < \nu \end{aligned} \qquad (3.10)$$

θ varies from 1 to 10^{-4} depending on crystal purity.

Wakayama and Williams have been able to account for the observed flourescence quenching using the pair state model.

The fact that quenching of delayed flourescence by injecting carriers is observed indicates that exciton carrier interactions will affect the quantum efficiency of electroluminescence.

3.3 Exciton-surface Interactions

The interaction of excitons with a crystal surface may result in the quenching of the exciton. The quenching mechanism at the boundary between an organic semiconductor and an electrode consists of either a charge transfer or an energy transfer process. An exciton can transfer an electron to a trapping centre at the surface producing a free hole in the semiconductor or an exciton can transfer its energy to the acceptor molecules present at the surface.

Williams, Adolf and Schneider [45] have measured the monomolecular decay constant, β, as a function of crystal thickness. After excitation by a helium-neon laser the exciton lifetime (β^{-1}) was determined from the relationship $I_F \alpha \exp(\frac{2t}{\tau})$, where τ is the triplet lifetime. The crystal thickness was found to have a large effect on the triplet lifetime. Figure 3.2 shows the result as obtained by Williams et al.

The concentration of triplet excitons in a thick crystal may be described by

$$\frac{d[T]}{dt} = - \beta[T] + \gamma[T]^2 \qquad (3.11)$$

where as before β is the unimolecular triplet decay constant and γ is the bimolecular triplet decay constant. If the decrease in triplet lifetime experimentally observed is due to diffusion of excitons to the surface followed

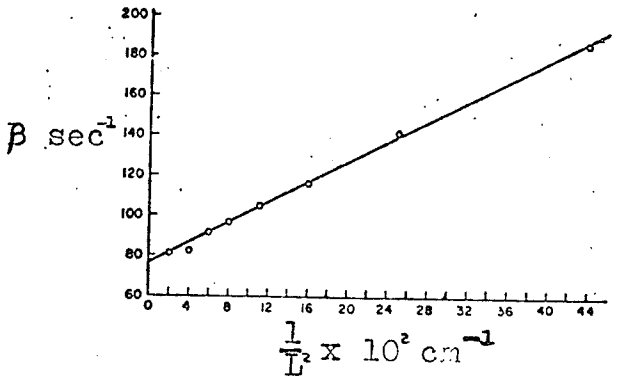

Fig. 3.2 The monomolecular triplet decay constant as a function of $1/L^2$. L is the crystal thickness. (After Williams et al [45].)

by surface quenching then equation (3.11) becomes

$$\frac{d[T]}{dt} = - \beta[T] - \gamma[T]^2 + D \frac{d^2[T]}{dx^2} \tag{3.12}$$

where D is the diffusion constant in the x direction. Assuming complete surface quenching (that is $[T\ (x = 0, L)] = 0$), weak excitation and a uniform initial triplet density ($[T\ (t = 0, x)]$ = constant), the solution of equation (3.12) was shown by Kepler and Switenelick [21] to be

$$[T\ (x, t)] = \frac{4}{\pi} [T]_o \sum_{k=o}^{\infty} \frac{1}{2k+1} \exp \{-[\beta + \frac{(2k+1)^2 \pi^2 D}{L^2}]t\} \sin \frac{2k+1}{L} \pi x \tag{3.13}$$

where L is the crystal thickness and β' the reciprocal of the actual lifetime. For time large enough

$$[T] = \frac{4}{\pi} [T]_o \exp (-\beta' t) \sin (\frac{\pi x}{L}) \tag{3.14}$$

where

$$\beta' = \beta + \frac{\pi^2 D}{L^2} \tag{3.15}$$

since the $k=o$ term dominates. The reciprocal lifetime has been plotted as a function of $\frac{1}{L^2}$ in Figure (3.2). It should be noted that the diffusion constant of the triplet exciton can be obtained from the slope of the curve. It should also be noted that a change in triplet lifetime from the bulk value first becomes apparent with a crystal thickness of 750-1000μ. For crystals thicker than this surface quenching of triplet excitons can be ignored.

CHAPTER IV

ELECTROLUMINESCENCE IN ANTHRACENE CRYSTALS

Electroluminescence in anthrance crystals using a pair of double injection electrodes has in recent years become a well known phenomenon. The fact that different materials used for electrodes result in different threshold voltage for the appearance of electroluminescence indicates that each such material in contact with the crystal surface will form a different potential barrier for carrier injection. This also implies that there are no perfect ohmic contacts.

The interface between an electrode and a crystal surface is never uniform. Thus there must exist microregions at which the potential barrier has a profile more favourable to carrier injection than that at other regions of the interface. The current density passing through a crystal is therefore filamentary and not uniform as has often been assumed. The current filaments formed in such materials as S_i and G_aA_s have been observed by Barnett et al. [6].

Hwang and Kao [19] have developed a theoretical model for filamentary injection and have used it to investigate some aspects of the electroluminescence in anthracene crystals.

The following assumptions are made in the analysis of filamentary double injection.

(1) At voltagesabove the threshold voltage more than one filament may be formed between the electrodes. However, for simplicity, it is assumed that only one filament is formed which is located along the z-axis of a cylindrical co-ordinate system. The effective radius of the filament is r_d.

(2) In the filament the longitudinal component of the diffusion current can be ignored because of the large longitudinal electric field and the radial component of the drift current can be ignored because of the small radial field.

(3) The free electron and hole densities follow the Maxwell-Boltzmann statistics, while the trapped electron and hole densities follow the Fermi-Dirac statistics.

(4) The mobility of the free electrons, μ_n, and that of the free holes μ_p are not affected by the presence of traps and the electric field.

(5) The hole injecting contact is at $z=0$ and the electron injecting contact is at $z=d$, the sample thickness being d.

(6) The recombination rate R consists of a longitudinal component R_z and a radial component R_r.

The behaviour of double injection in a crystal is governed by the current flow equations.

$$J_n = J_{nz} + J_{nr}$$

$$= q\mu_n n_f E \hat{i}_z + qD_n \left(\frac{dn_f}{dr}\right)\hat{i}_r \tag{4.1}$$

$$J_p = J_{pz} + J_{pr}$$

$$= q\mu_p p_f E \hat{i}_z - qD_p \left(\frac{dp_f}{dr}\right)\hat{i}_r \tag{4.2}$$

$$J = J_n + J_p = J_z + J_r \tag{4.3}$$

the continuity equations

$$\mu_n \left(\frac{d}{dz}\right) n_f E = - \mu_p \left(\frac{d}{dz}\right) P_f E = R_z \tag{4.4}$$

$$\frac{D_n}{r} \frac{d}{dr} \left(r \frac{dn_f}{dr}\right) = \frac{D_p}{r} \frac{d}{dr} \left(r \frac{dP_f}{dr}\right) = R_r \tag{4.5}$$

and the Poisson equation

$$\nabla \cdot E = \frac{q}{\varepsilon} [P_f + P_t - n_f - n_t] \tag{4.6}$$

where n_f and p_f are the densities of free electrons and holes and p_t and n_t are the densities of trapped electrons and holes. J, J_n and J_p are the total, the electron and the hole current densities, respectively; E is the applied electric field; ε is the permittivity of the crystal; and D_n and D_p are the diffusion coefficients for the electrons and holes.

In the case of traps confined to a single discrete energy level the current density is given by

$$J_z(r) = J_{zo} [1 + (\tfrac{1}{6} \lambda_a J_{zo})^{\frac{1}{2}} r]^{-2} \tag{4.7}$$

where λ_a is a constant depending on the physical properties of the crystal, and

$$J_{zo} = \frac{q}{8} \varepsilon \mu_{eff} \frac{U^2}{d^3} \tag{4.8}$$

which is the normal result for space charge limited currents with the effective carrier mobility μ_{eff}.

In the case of traps distributed exponentially within the forbidden energy gap the current density is given by

$$J_z(r) = J_{zo} \overline{W}_b \tag{4.9}$$

where

$$\overline{W}_b = \exp\left[-\left(\lambda_b J_{zo}^{\frac{1}{2}}\right)^{\frac{1}{2}} r\right] \qquad \text{for } \ell=2$$

$$= \left[1 + \left(\frac{2-\ell}{2\ell}\right)\left(\frac{2\ell\lambda_b J_{zo}^{\frac{1}{2}}}{2+\ell}\right)^{\frac{1}{2}} r\right]^{-\frac{2\ell}{(2-\ell)}} \qquad \text{for } 1<\ell<2 \text{ and } \ell<2 \tag{4.10}$$

and

$$J_{zo} = q^{\ell-1}\,\mu'_{eff}\left(\frac{2\ell+1}{\ell+1}\right)^{\ell+1}\left(\frac{\ell\varepsilon}{\ell+1}\right)^{\ell}\frac{V^{\ell+1}}{d^{2\ell+1}} \tag{4.11}$$

In the case that more than one filament exists the total current is simply the sum of the currents in each filament.

In molecular crystals the electron and hole mobilities are small and the recombination rate constant is large. Thus, there is a small space charge overlap and the simultaneous injection of electrons and holes will produce two space charge limited currents within the filament. Electroluminescence occurs when the two charge fronts meet and recombine radiatively.

The electroluminescence brightness is governed by the external quantum efficiency given by [19]

$$\eta_q = \eta_i\,\eta_g\,\eta_e = \eta_{int}\,\eta_e \tag{4.12}$$

where η_i is the carrier injection efficiency which is the ratio of the minority carrier current to the total current and η_g is the light generation efficiency. η_{int} is the internal quantum efficiency which is a function of the total current density and temperature. η_e is the light extraction efficiency which is defined as the ratio of the light transmitted power to the power lost in the bulk and at the surface. This quantity can be considered constant for any given sample.

The electroluminescence in molecular solids results from the recombination of injected electrons and holes to yield singlet and triplet excitons. The singlet excitons producing florescence are generated either by direct electron-hole generation or indirectly by the triplet-triplet annihilation as described earlier.

The electroluminescent intensity will depend on the efficiency of generating the S_{dir} and S_{ind} and consequently their population in the crystal. The number of singlet excitons generated directly per unit volume per unit time is given by [14, 19]

$$G_s = \frac{g_s J_z(r)}{q\lambda_s} \tag{4.13}$$

where λ_s is the diffusion length of the singlet exciton and g_s is the fraction of the electron-hole pairs that produce direct singlet excitons (approximately ¼ for anthracene [14]). Hwang and Kao [19] have shown that the brightness of the prompt electroluminescences is given by

$$B = b_1 I \tag{4.14}$$

where b_1 is a constant and I is the total current.

The number of triplet excitons generated per unit volume per unit time is given by [14, 19]

$$G_T = \frac{g_T J_z(r)}{q\lambda_T} \tag{4.15}$$

where λ_T is the diffusion length of the triplet exciton and g_T is the fraction of electron-hole pairs that produce triplet excitons after recombination (approximately $\frac{3}{4}$ for anthracene). In the low injection or low current case it has been shown that the delayed electroluminescence brightness is given by

$$B = b_3 \int_o^{r_d} J_z^{\,2}\,(r)\,dr \tag{4.16}$$

where b_3 is a constant. In the high injection or high current case

$$B = b_5 I \tag{4.17}$$

where b_5 is a constant.

In the steady state the brightness of the electroluminescence is the sum of the prompt and delayed electroluminescence. In the low current case we then have

$$B_T = b_1 I + b_3 \int_o^{r_d} J_z^{\,2}\,(r)\,dr \tag{4.18}$$

In the high current case we have

$$B_T = b_1 I + b_5 I \tag{4.19}$$

For the high current case the brightness is proportional to current whereas for the low current case if $b_3 > b_1$ then the brightness becomes proportional to I^2. Figure (4.1) shows that these theoretical results by Hwang and Kao agree well with experimental results obtained from several sources.

Using equations (4.7), (4.9), (4.18) and (4.19) the voltage dependence of the electroluminscence brightness can be obtained. Using properly chosen parameters Hwang et al. have been able to obtain good agreement with experiments [19]. Their results are shown in Figure (4.2).

The temperature dependence of the electroluminescent intensity as obtained by Hwang et al. [18, 19] is shown in Figure (4.3). This phenomena may be explained in terms of exciton carrier interactions [13, 40, 41] and the temperature dependence of the current. As the temperature is

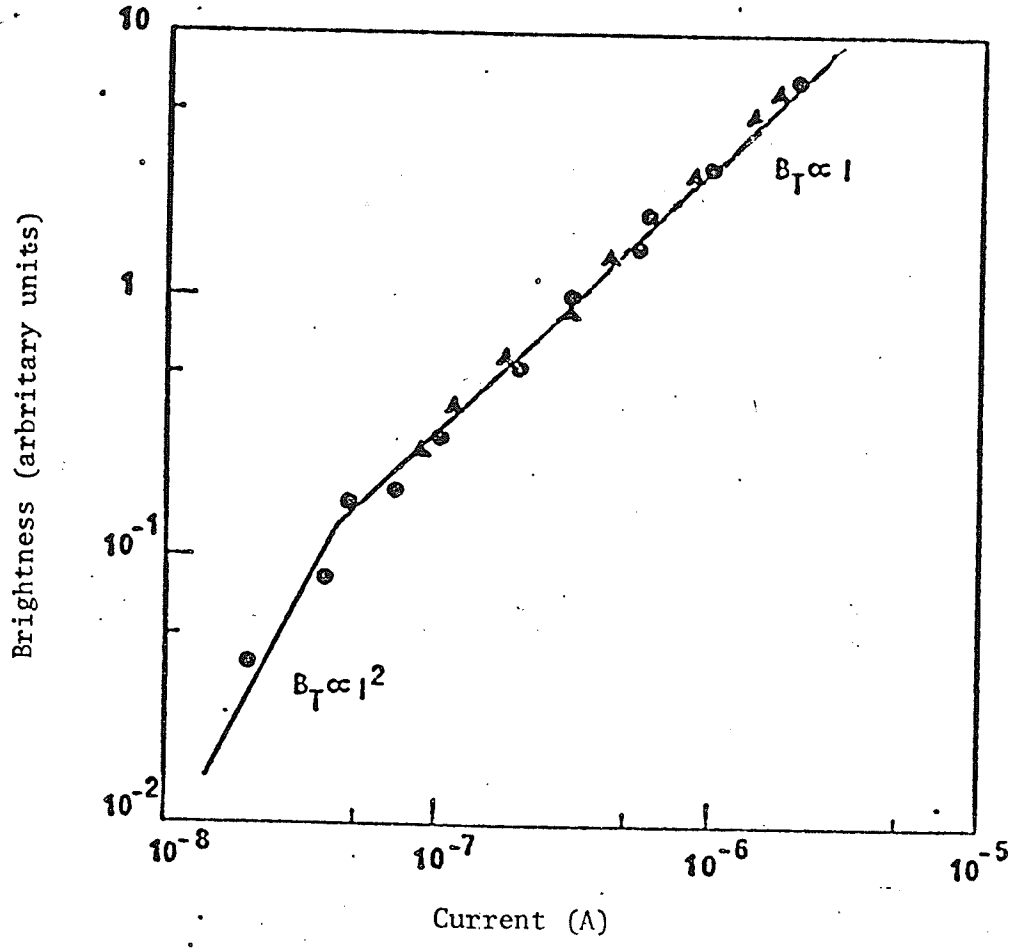

Fig. 4.1 Electroluminescent brightness as a function of current for undoped anthracene crystals. Solid line is based on the theory (after Hwang and Kao [19]) and experimental results are after William and Schadt▲[48], Hwang and Kao●[19].

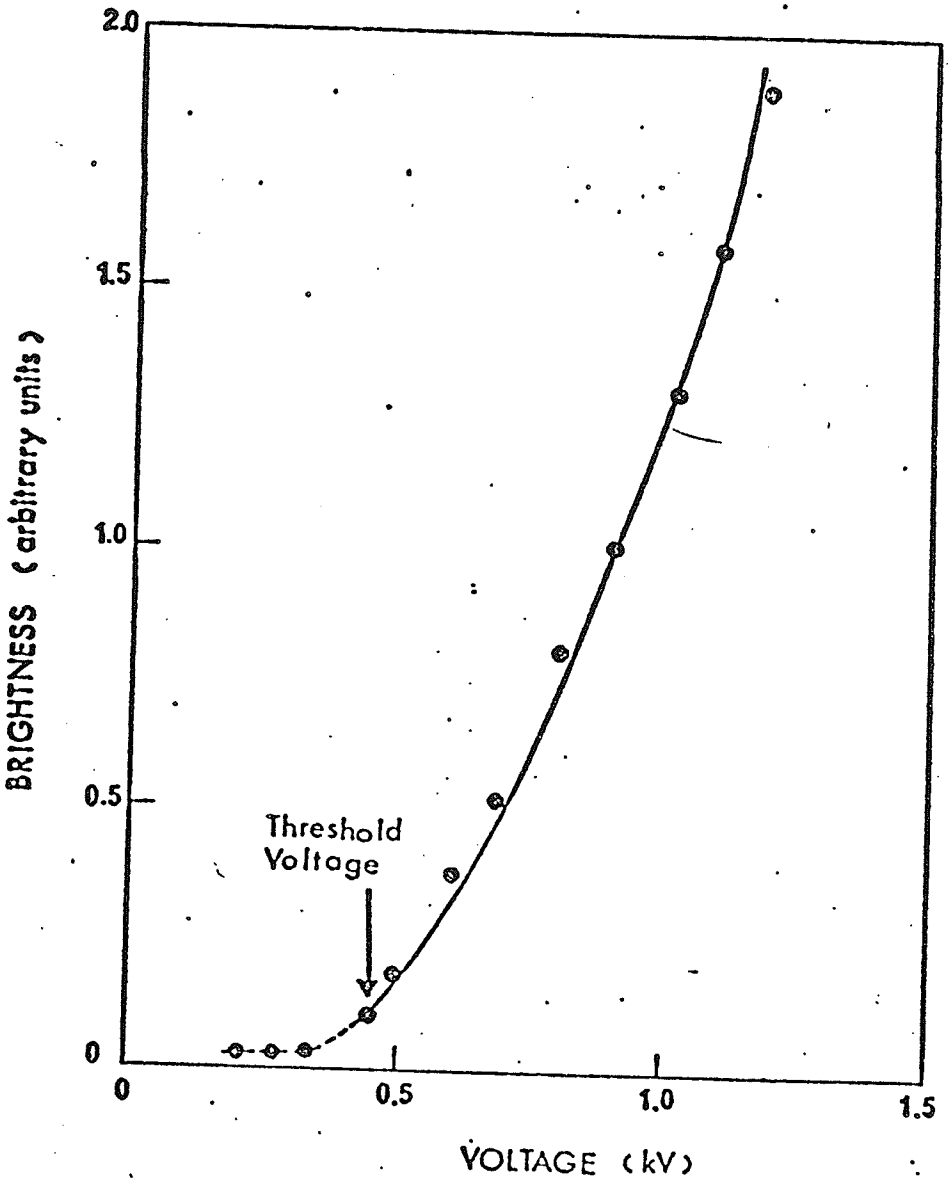

Fig. 4.2 Electroluminescent brightness as a function of applied voltage for undoped anthracene crystals at 20°C. (After Hwang and Kao [19].)

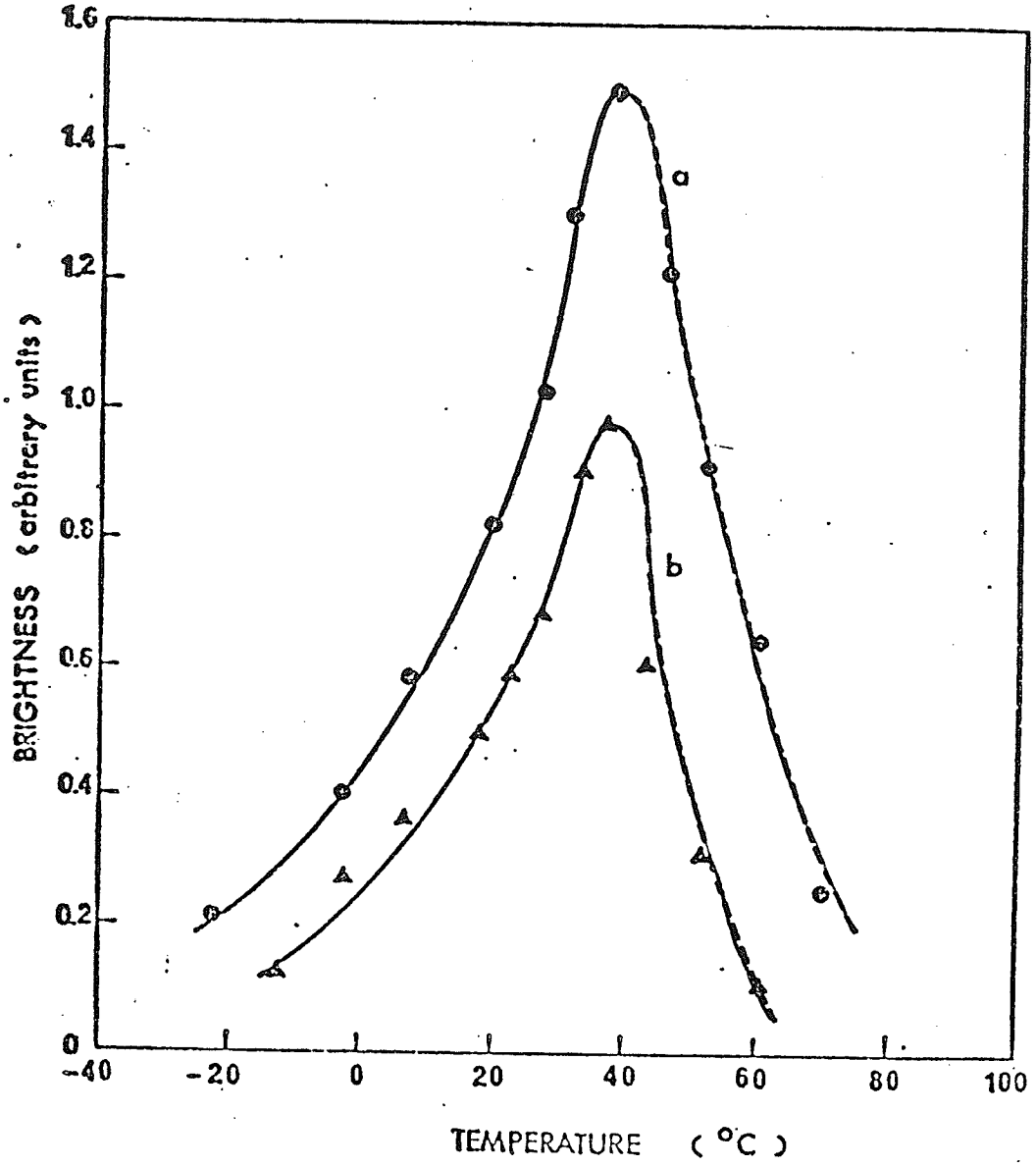

Fig. 4.3 Electroluminescent brightness as a function of temperature for undoped anthracene crystals for (a) applied voltage: 1.2 kv, and (b) applied voltage: 1.0kv using two evaporated silver contacts. (After Hwang and Kao [19].)

increased the current will also increase thus giving a larger carrier injection efficiency. As the current increases, however, there is a corresponding increase in the interaction of excitons with charge carriers. The presence of these two competing processes results in the observed peak.

CHAPTER V

EXPERIMENTAL PROCEDURES

5.1 Sample Preparation

The anthracene crystals used were supplied by the Harshaw Chemical Company. The bulk anthracene was cleaved along the a-b plane producing crystals two or three mm in thickness. It was not possible to obtain crystals of less thickness through cleavage without breaking the sample. The sample was then reduced to the desired thickness by initially cutting off very thin layers using a very sharp knife. In order not to damage the sample by overheating or introducing lattice dislocations the sample was reduced to its final thickness by polishing very slowly on lens paper covered with pure benzene. The thickness of the samples used was approximately .4 mm. A small glass ring of 5 mm diameter and approximately 4 mm length was epoxied to the crystal surface. To ensure that the glass ring was clean it had been washed in water, dried and boiled in benzene. A silver wire electrode was also boiled and attached to the glass ring in contact with the crystal surface.

5.2 Electrode Preparation

In many experiments such as electroluminescence and studies of conduction processes the type of electrode used is of great importance, often determining whether the experiment can be performed. The most important characteristic of an electrode is usually, the number and type of carrier it is capable of injecting into the crystal under the experimental conditions. The most important factor determining the characteristics of the electrode is the difference between the fermi level of the electrode material and the conducting states in the crystal. An often used method

of determining this barrier height is photoemission. The dependence of the photocurrent on the incident photon energy is measured. When the photon energy is equal to the barrier height a large incease in photocurrent is observed. Figure 5.1 shows the barrier height for emission of holes and electrons from various metals into anthracene.

Metal	Φ_B^+	Φ_B^-
Ag	1.20	----
Al	1.86	----
Au	1.17	----
Ca	----	1.07
Ce	2.20	1.52
Mg	1.97	1.75
Na	----	1.00
Pb	1.80	1.92
Pt	0.89	----

Figure 5.1 Barrier Height for Photoemission

Silver has a barrier of 1.20 eV for the emission of holes into the valence band of anthracene. Sodium has a barrier of 1.0 eV for the emission of electrons into the first conduction band of anthracene. We have chosen these metals for our electrodes.

If an alkali metal is deposited on an anthracene crystal the contact with the anthracene surface will not be the metal but the blue alkali-anthracenide charge transfer complex. Since sodium metal cannot be evapor-

ated because of its chemical reactivity we have prepared a solution of the charge transfer complex. Good injecting contacts were obtained when a very concentrated solution of sodium and anthracene in tetrahydrofuran was brought into contact with the crystal. The solvent was slowly evaporated until the electrode became solid. Great care must be taken in producing these contacts. Complete removal of oxygen, water vapour and other materials which would interact with the solution is necessary. Figure 5.2 shows the apparatus which was used to prepare the solution. Sodium metal reacts with oxygen to produce sodium peroxide ($Na_2\ O_2$) and reacts vigorously with water to produce sodium hydroxide (Na OH) and hydrogen. We thus can use sodium to remove the oxygen and water dissolved in the organic solvent, tetrahydrofuran. The procedure for producing the solution will now be described.

5.2.1 Purifying the Solvent

(a) Approximately 5 to 10 ml of the solvent is placed in vessel A. The vessel is attached to the vacuum line by means of a ground glass joint. The solvent is solidified using liquid nitrogen and the valve is opened to evacuate the vessel to 10^{-5} torr.

(b) Because sodium reacts with oxygen it is normally stored and handled under benzene. The oxidized surface layer is cut from a small piece of sodium. This is done under benzene to protect the new surface. The sodium is then quickly transferred to vessel B which is then pumped down to 10^{-5} torr. In order to supply a large reaction surface the sodium is heated until it evaporates forming a sodium mirror on the inside wall of the vessel (with the valve closed).

(c) The vessel is now cooled with liquid nitrogen and the solvent is distilled from vessel A to vessel B. Vessel A is removed and rinsed

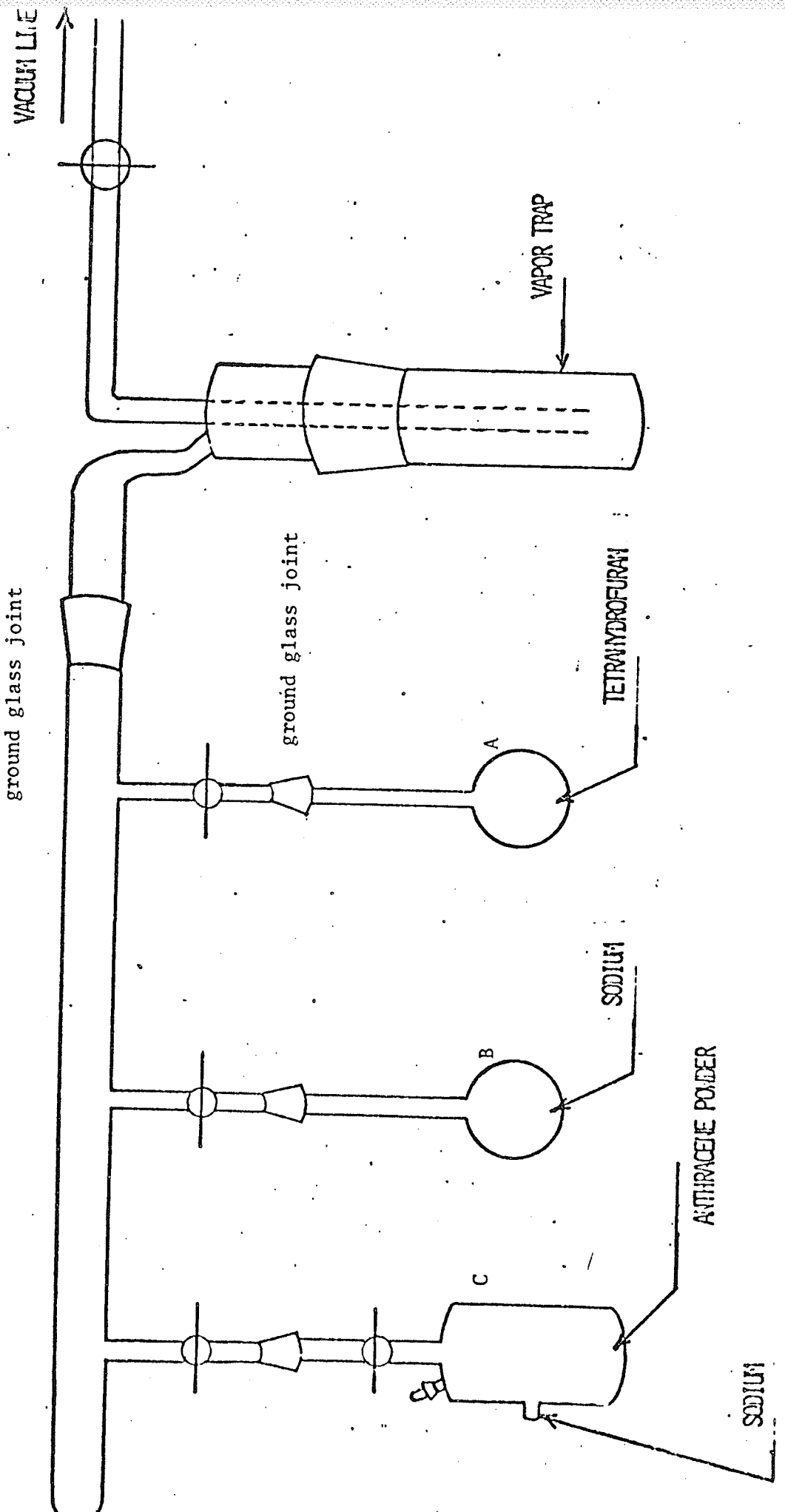

Fig. 5.2 Apparatus for producing electrode solution

with pure acetone. After the vessel is allowed to dry process (b) is repeated with the solvent being distilled back into vessel A.

(d) The solvent is distilled repeatedly under sodium metal until the solid solvent becomes slightly bluish in colour. This normally requires four or five distillations. With the first distillation it is noticed that the sodium mirror, initially silver in colour, becomes quite greyish. This is the result of the formation of sodium hydroxide. After a few distillations, the sodium mirrors are no longer affected.

(e) Water can be effectively used to remove the reaction products from a vessel which has been used in a purification cycle. A little caution is required since the reaction is quite vigorous. The vessel is then rinced with pure acetone, allowed to dry and can be used in the next cycle.

5.2.2 Producing the Solution

(a) Anthracene powder or small pieces of bulk anthracene with freshly cleaved surfaces is introduced into vessel C. A small piece of sodium is then inserted and the vessel is evacuated to 10^{-5} torr. The sodium is heated to form a sodium mirror and the purified solvent is distilled into vessel C. The contents of the vessel are heated to form a concentrated solution of sodium and anthracene in tetrahydrofuran. The solution actually contains sodium anthacene ion pairs since the sodium has produced the anthracene negative ion.

5.2.3 Formation of the Electron Injecting Contact

The sealed vessel is transferred to the vacuum system as shown in Figure 5.3. The vacuum system is thoroughly flushed with Argon. Two or three drops of the solution are dropped onto the crystal surface inside the small restraining ring. The solvent is allowed to slowly evaporate until the electrode is solid. A protective layer of parafin wax is applied

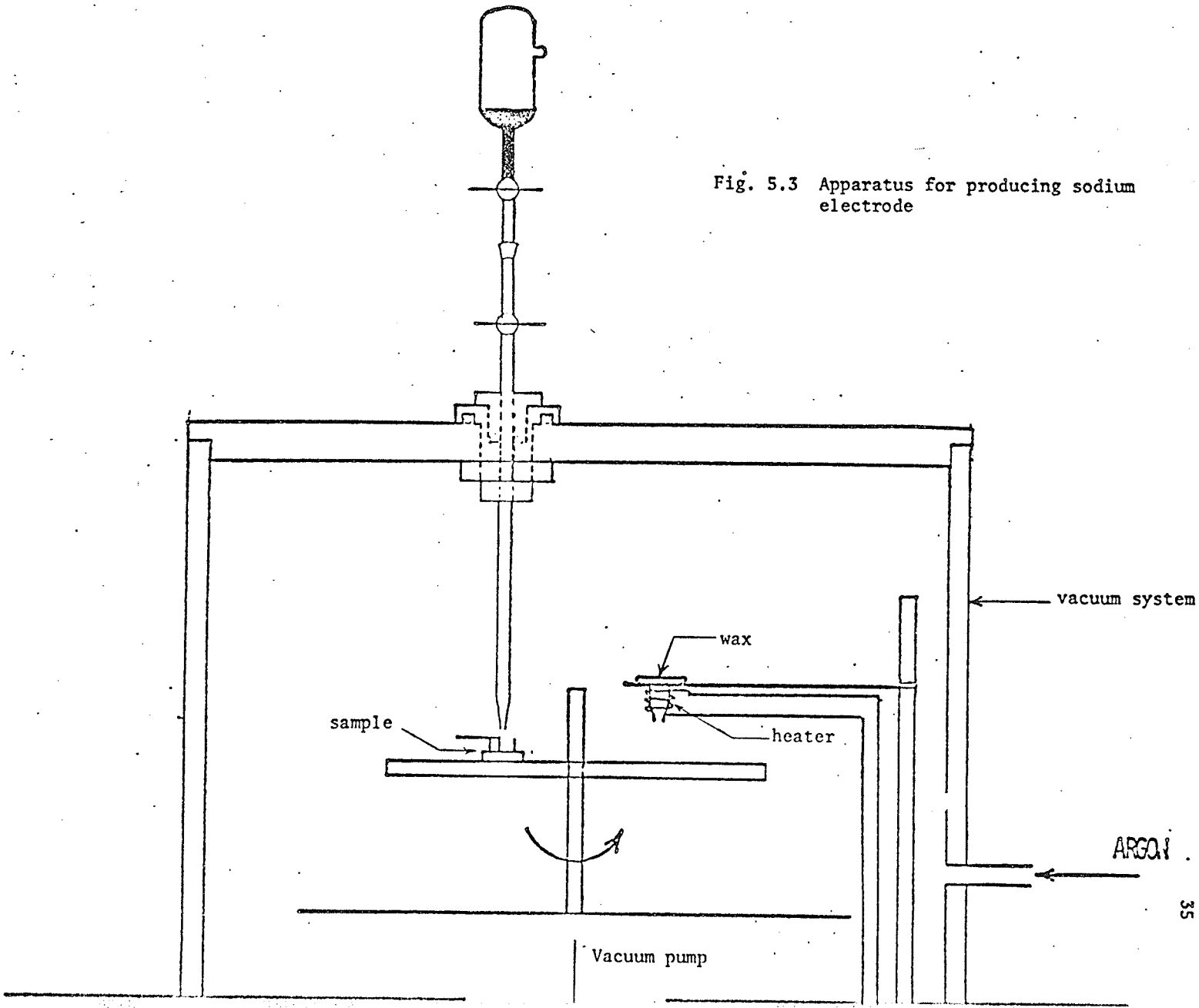

Fig. 5.3 Apparatus for producing sodium electrode

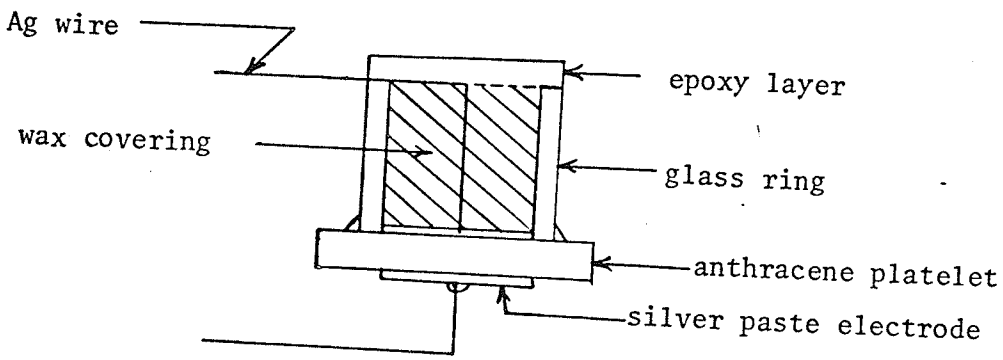

Fig. 5.4 Electroluminescent diode

as shown in Figure 5.3 The sample is then removed from the vacuum system and a layer of epoxy is applied to protect the electrode. Figure 5.4 shows the structure of the electroluminescent diode.

5.3 Measurement Technique

Figures 5.5 and 5.6 show the amplifiers used to obtain a high a.c. voltage and a high half-wave rectified a.c. voltage respectively. An audio step-up transformer proved unsatisfactory for this purpose because of the restricted bandwidth for which one could obtain the required high voltage.

In both cases the sample was connected directly to the amplifier output without a current limiting resistor. The input to each amplifier was supplied by a General Radio Company 1310 oscillator. To obtain a rectified a.c. output from the second amplifier a diode was introduced into the input circuit. To ensure that the output was uni-directional a variable voltage supply in series with a resistor was connected across the output. The voltage could be adjusted to produce the proper d.c. level. The output coupling capacitor as well as isolating the sample from the biasing circuit also produced a d.c. level shift between the input and the output (see waveforms in Figure 5.6).

Figure 5.7 shows the measurement circuit used. Since the brightness measured was in arbritary units the position of the sample with respect to the photomultiplier as well as the photomultiplier voltage must be kept constant throughout the experiment. The sample was placed in an Associated Testing Laboratories Inc. model ELH-2LC-1 environmental chamber in front of a viewing port to which the photomultipler was connected. The environmental chamber, photomultiplier housing as well as the connecting light passage was opaque allowing the

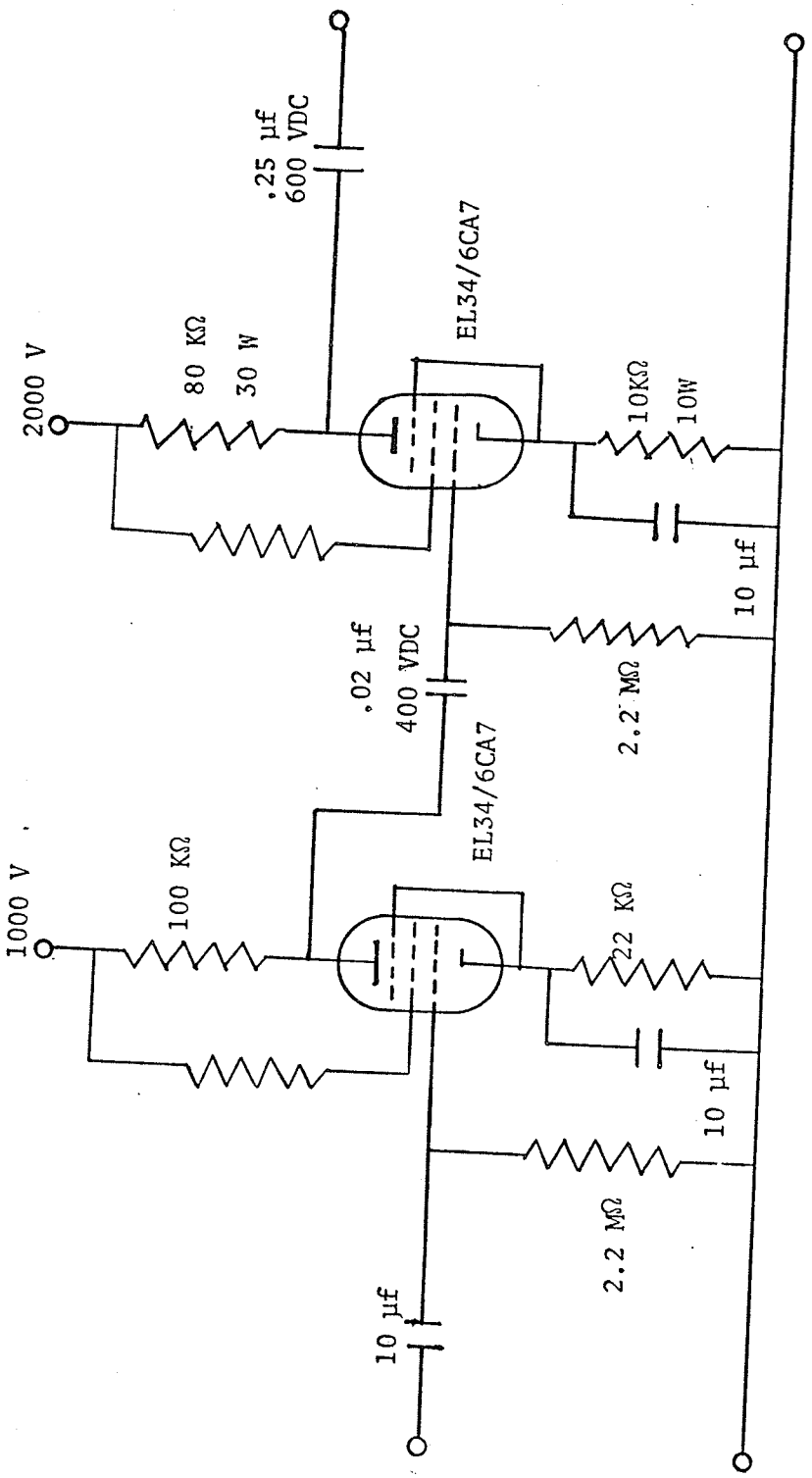

Fig. 5.5 Amplifier used to produce high a.c. voltage

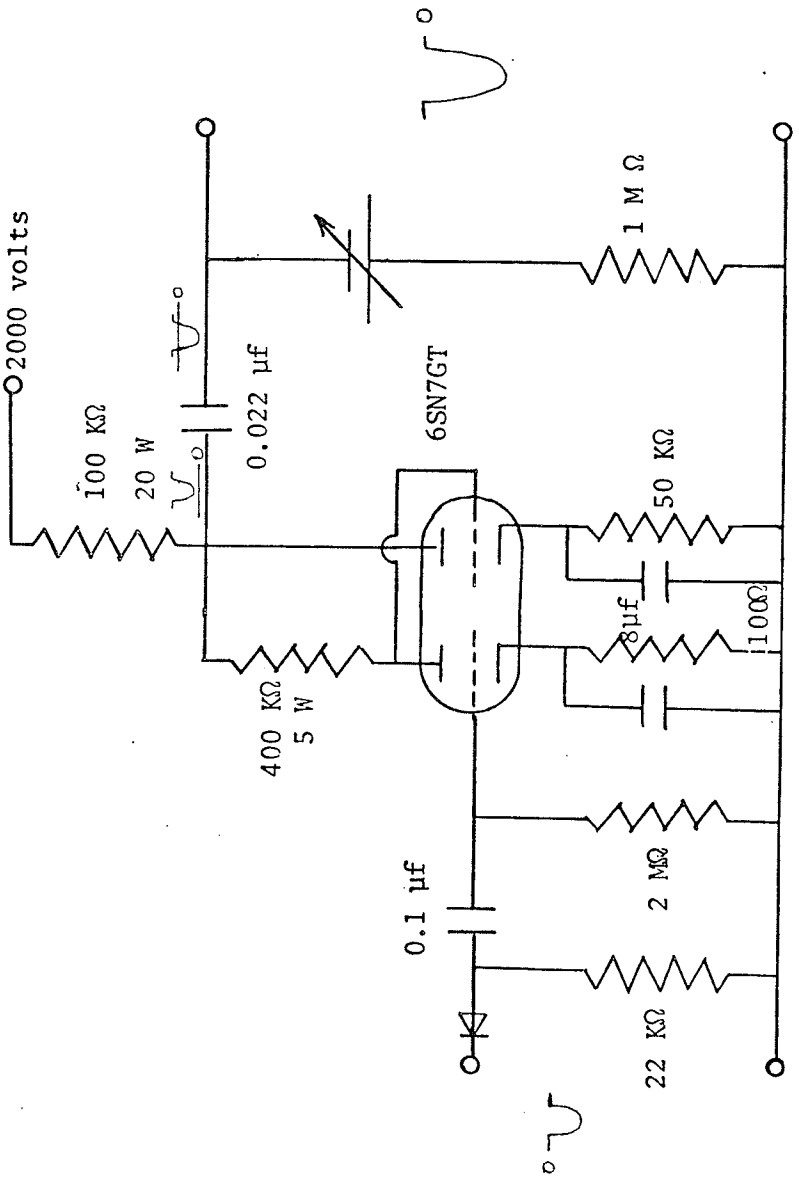

Fig. 5.6 Amplifier used to produce large half wave rectified voltage

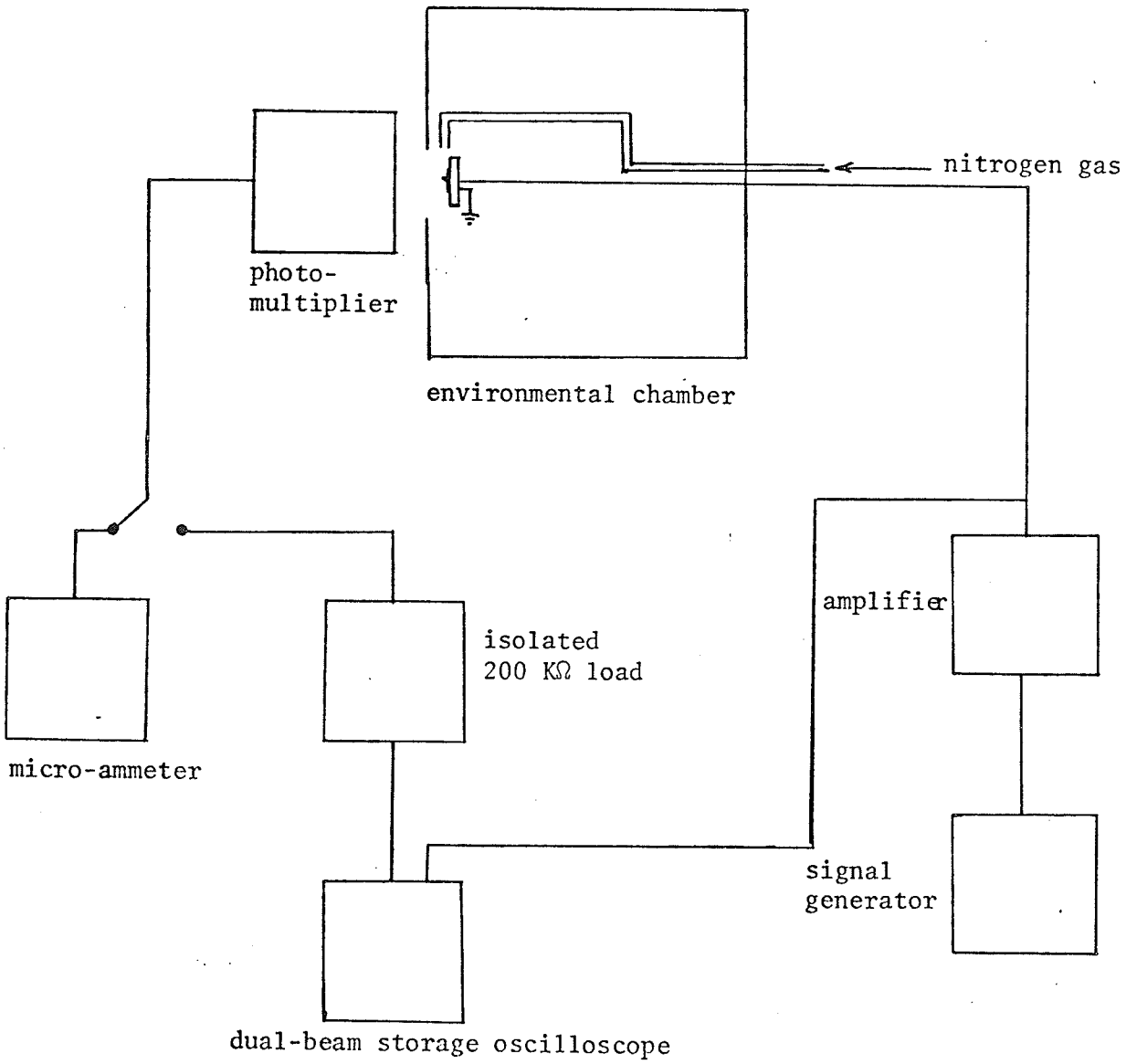

Fig. 5.7 Measurement circuit

the experiment to be done under normal lighting. The photomultiplier tube must also be thermally isolated from the environmental chamber since any fluctuation in the temperature of the photomultiplier results in a change in the photomultiplier response to a given light intensity. The temperature of the environmental chamber can be raised with a heating filament or decreased with the expansion of compressed carbon dioxide gas. Because the atmosphere in the environmental chamber cannot be controlled and simply consists of air, when the temperature was lowered nitrogen gas was blown over the crystal to prevent the condensation of water vapour. The introduction of any foreign material upon the crystal surface could modify the electroluminescence brightness.

To measure the integrated light output a Hewlett-Packard model 425A DC micro volt-ammeter was used to record the photomultiplier current. To measure the time dependence of the electroluminescence brightness a Tektronix type 549 dual beam storage oscilloscope was used. In order to limit the noise present in the measurement only shielded cables and connections were used.

CHAPTER VI

EXPERIMENTAL RESULTS AND DISCUSSION

6.1 A.C. Electroluminescence

6.1.1 Frequency Dependence of the A.C. Electroluminescence

Figure 6.1 shows the peak brightness as a function of frequency. As the frequency increases from 20 Hz to 5 KHz the brightness decreases monotonically. The electroluminescence appeared only on the half cycle in which the silver electrode was positive and the sodium electrode was negative. The results were obtained at a peak to peak voltage of 1600 volts although the results were consistent for voltages up to 2400 volts. Even at a voltage of 2400 volts peak to peak no electroluminescence was observed during the half cycle in which the sodium electrode was positive and the silver electrode was negative.

Figure 6.2 shows the integrated light output obtained by measuring the photomultiplier output with a microammeter. The brightness decreases monotonically with increasing frequency in a manner similar to that for the peak brightness. The total light output at 20 Hz is approximately two order of magnitude less than the electroluminescent brightness measured with a d.c. voltage of 800 volts (equal to the peak value of the a.c. voltage).

6.1.2 Time Dependence of the Electroluminescence

The series of photographs in Figure 6.3 show that there is a delay time between the time when the voltage is applied and the time when the electroluminescence appears. The photographs were taken with the crystal temperature at approximately 40°C. Figure 6.4 shows the frequency dependence of the delay time. The delay time saturates at approximately 40 μsec at

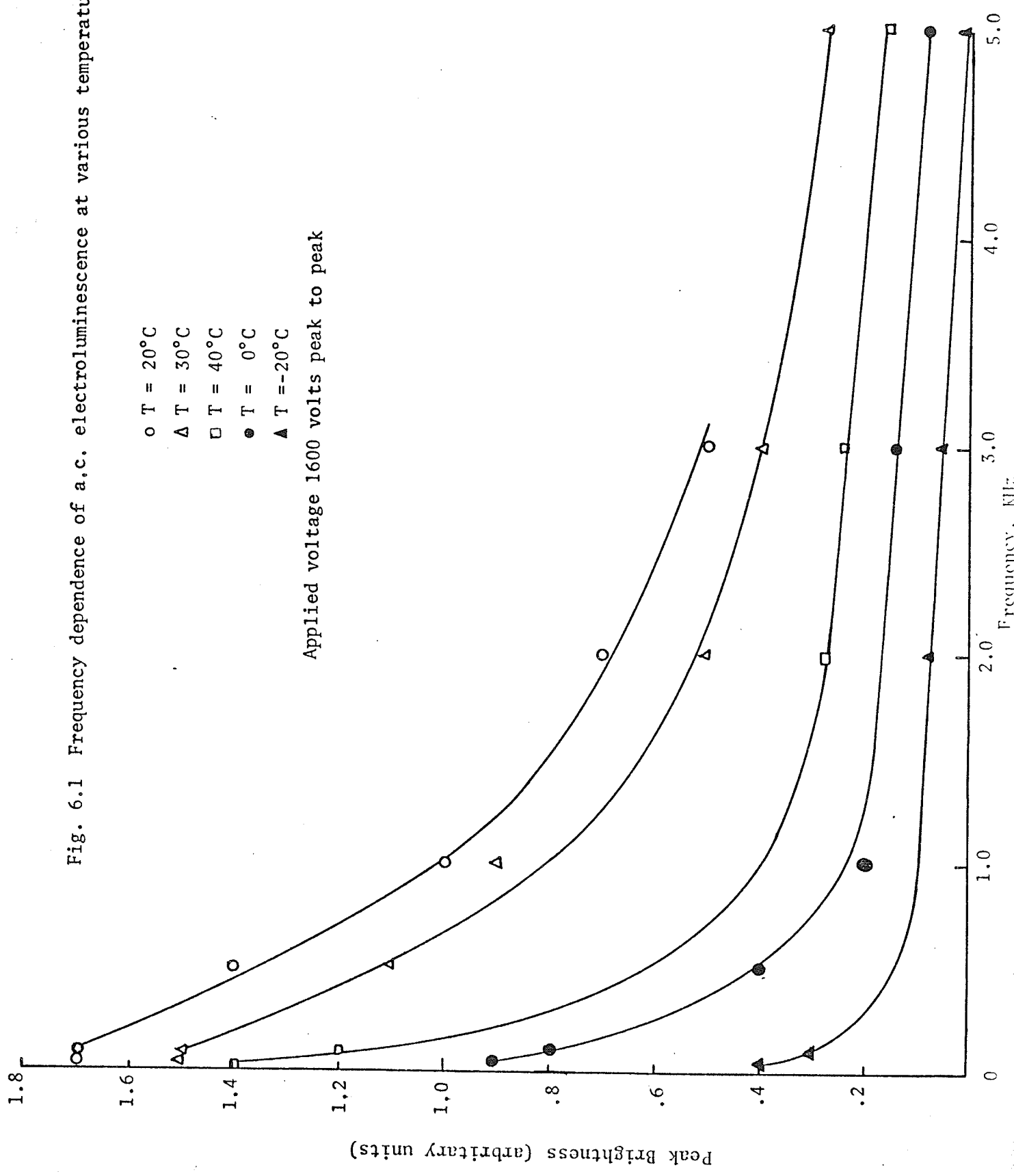

Fig. 6.1 Frequency dependence of a.c. electroluminescence at various temperatures.

Fig. 6.2 Frequency dependence of integrated electroluminescent brightness for various temperature.

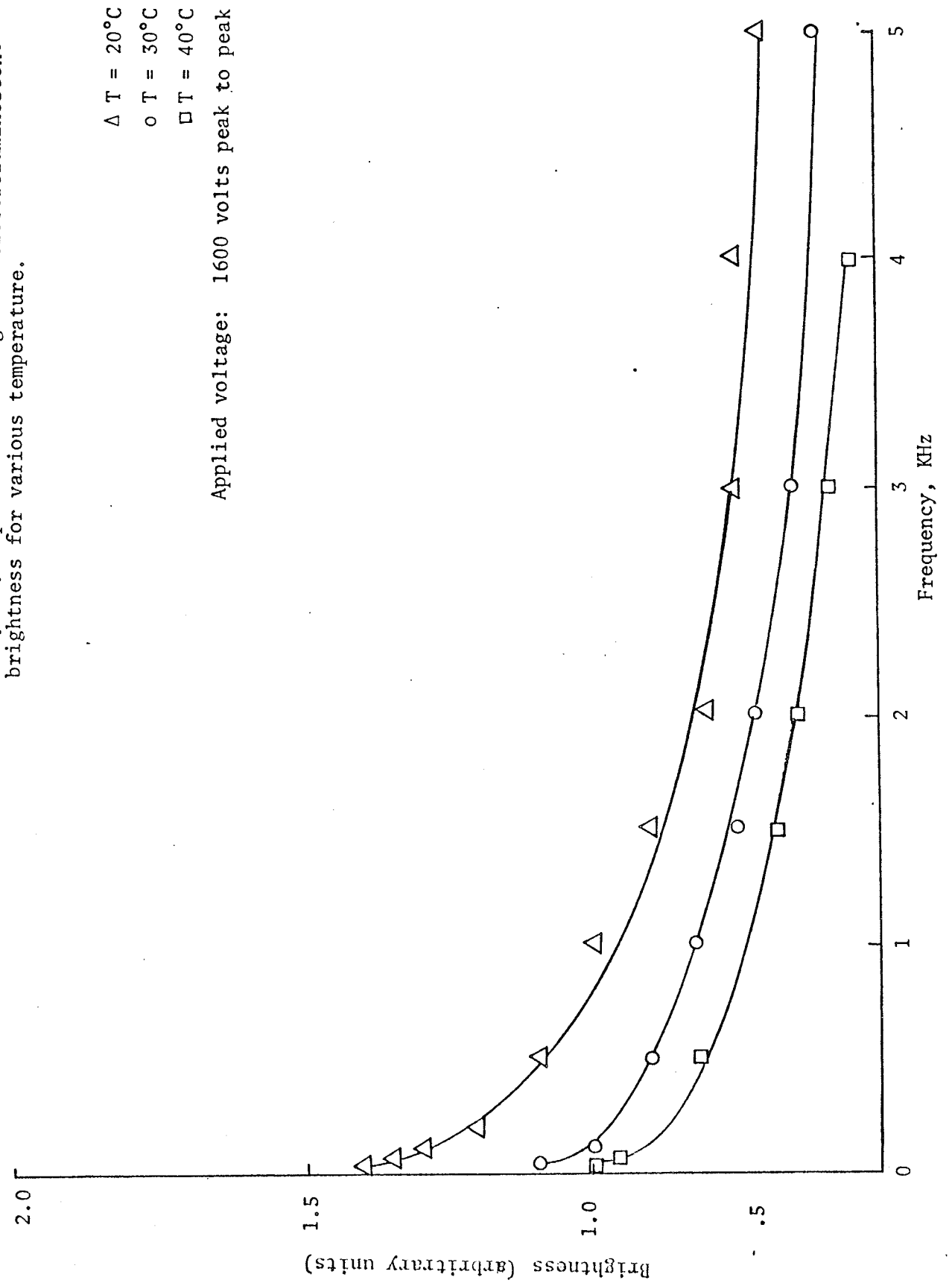

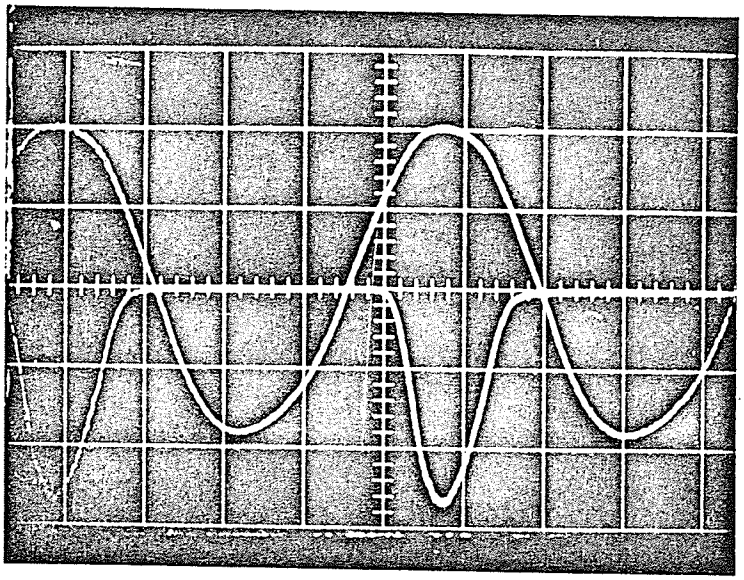

(a)

Scale: vert. voltage 400v/div
brightness .5v/div
horz. 10 msec/div

Frequency: 20 Hz

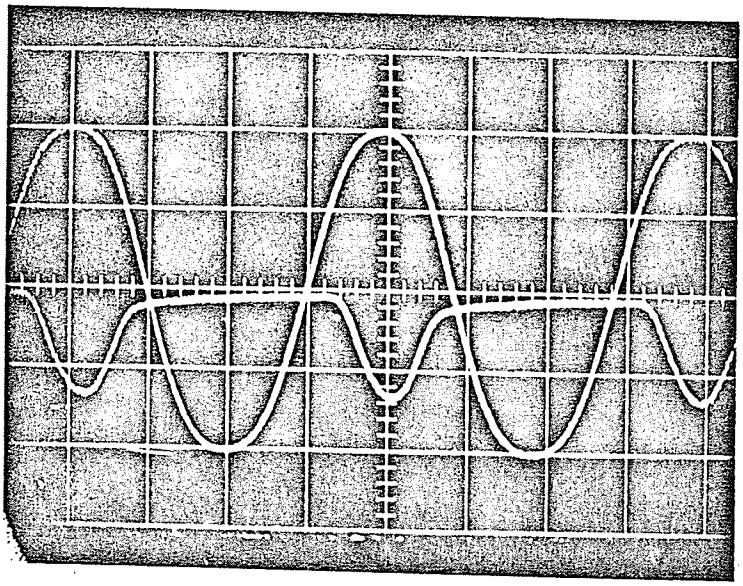

(b)

Scale: vert. voltage 400 v/div
brightness .5 v/div
horz. ,5 msec/div

Frequency: 500 Hz

Fig. 6.3 Time dependence of a.c. electroluminescence at various frequencies. The upper trace is the applied voltage and the bottom trace is electroluminescence brightness.

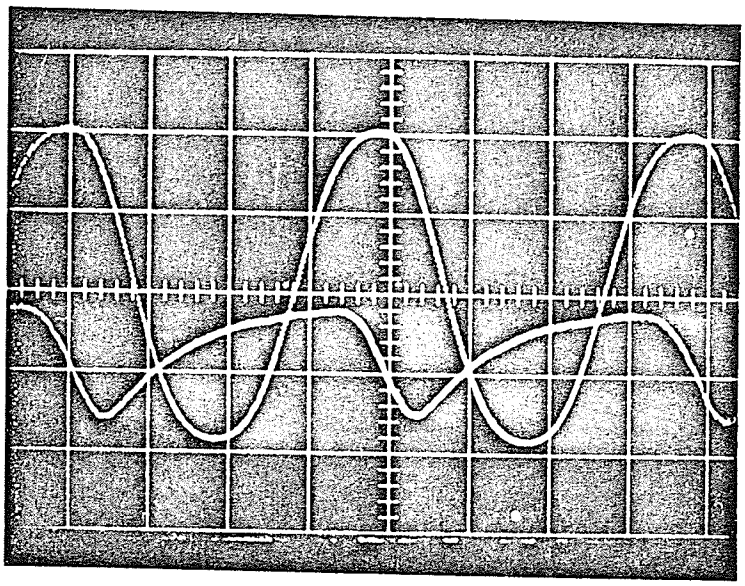

(c)

Scale: vert. voltage 400 v/div
brightness .1 v/div
horz. 50 μsec.div

Frequency: 5KHz

Fig. 6.3 Time dependence of a.c. electroluminescence. The upper trace is the applied voltage and the lower trace is the electroluminescence brightness.

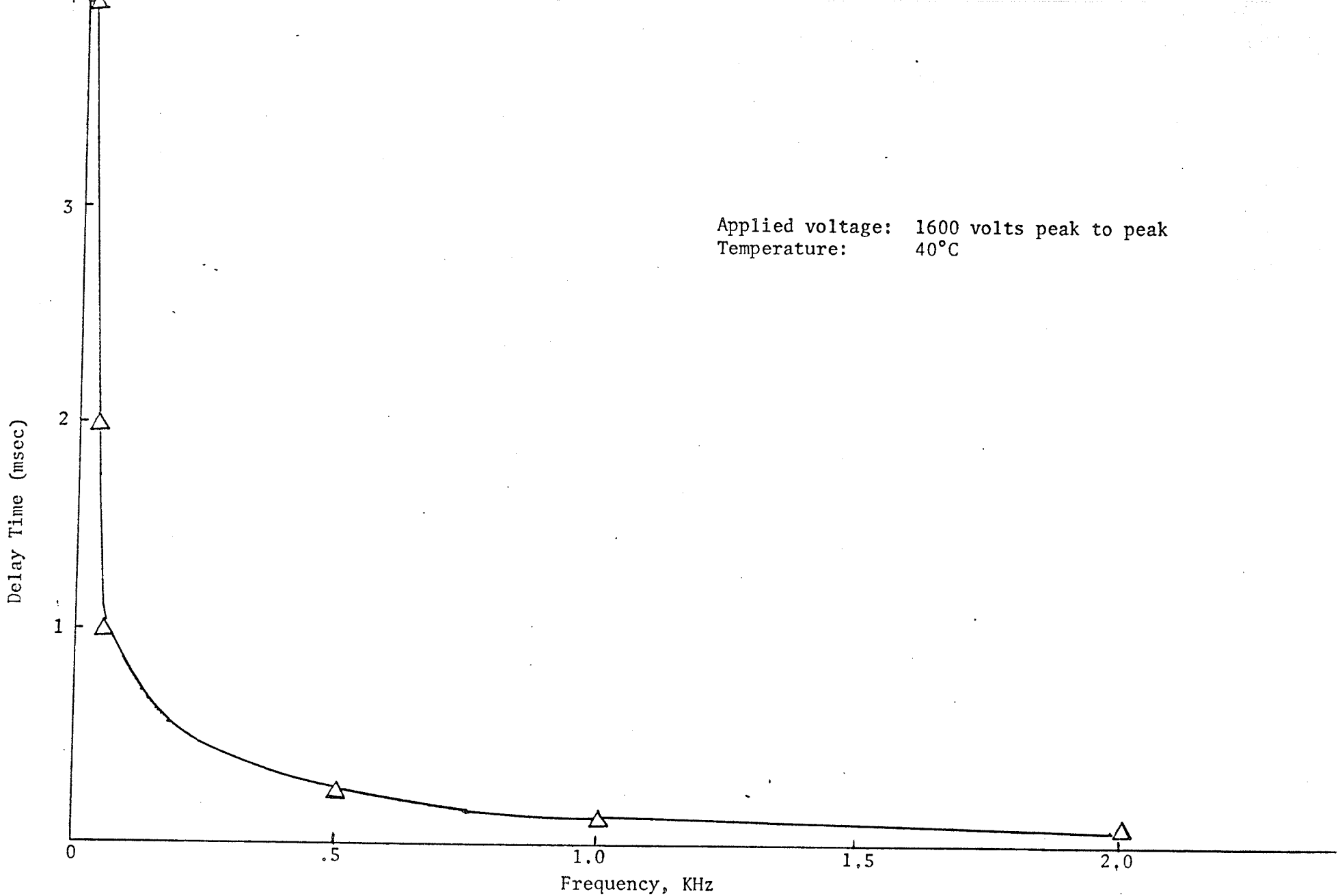

Fig. 6.4 Frequency dependence of delay time for appearance of electroluminescence

high frequencies. Figure 6.5 shows the rise and decay of the electroluminescence excited with a 800 volt rectangular pulse. The electroluminescence has a delay time of approximately 30 μsec.

An apparent frequency-dependent phase-shift exists between the peak electroluminescence brightness and the peak applied voltage. At 20 Hz no phase shift is apparent. As the frequency increases the phase shift increases. At 5 kHz the phase shift has become very noticeable.

The leading portion of the electroluminescence waveform is similar in shape to that of the applied voltage for all frequencies. At high frequencies, however, a significant exponential tail develops on the trailing edge as shown in Figure 6.3c.

6.1.3 Temperature Dependence of the Electroluminescence

Figure 6.6 shows the temperature dependence of electroluminescent brightness for temperatures between -20°C and 40°C at four fixed frequencies. The electroluminescent brightness increases with increasing temperature up to 20°C. Beyond this temperature the brightness decreases with increasing temperature. The temperature at which the peak occurs is practically independent of frequency for the range of frequencies used.

6.2 Electroluminescence Under a Half-Wave Rectified Voltage

6.2.1 Frequency Dependence of Electroluminescence

Figure 6.7 shows the frequency dependence of the peak electroluminescence brightness. The brightness decreases monotonically with increasing frequency in a manner similar to the a.c. electroluminescence. Electroluminescence appeared only if the applied voltage was of the proper polarity. The integrated light outout, at 20 Hz and at the applied voltage of 800 volts peak, was approximately one order of magnitude less than the

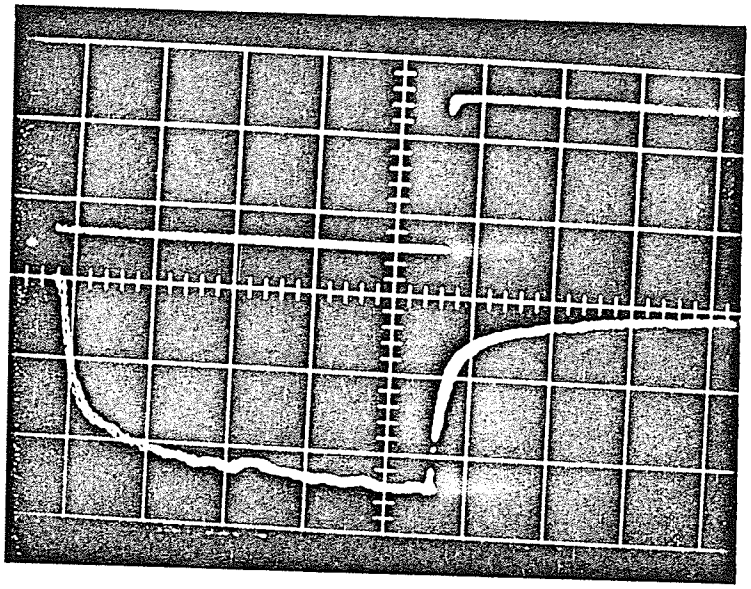

(a) Applied pulse

Scale: vert. voltage 400 v/div
brightness .1 v/div
horz. .5 msec/div

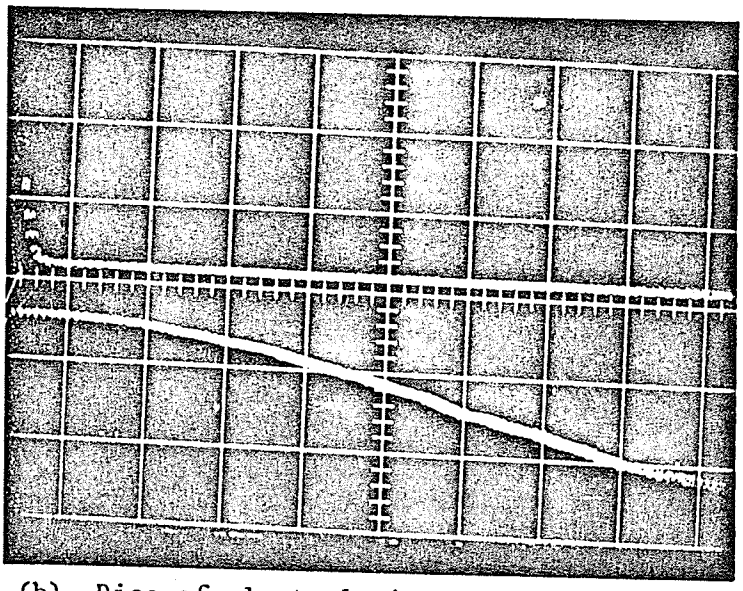

(b) Rise of electroluminescence

Scale: vert. voltage 400 v/div
brightness .05 v/div
horz. 20 μsec/div

Fig. 6.5 Electroluminescence with pulse excitation. The upper trace is the applied voltage and the bottom trace is the electroluminescence brightness.

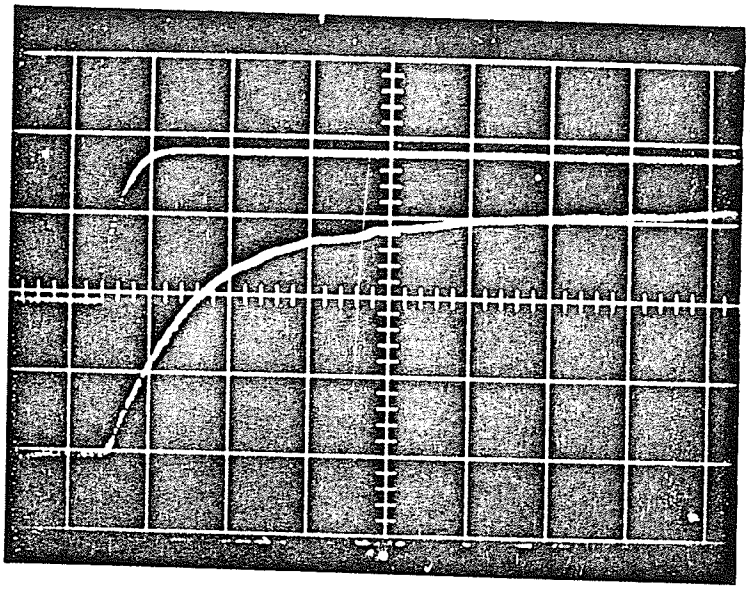

(c) Decay of electroluminescence

Scale: vert. voltage 400 v/div
brightness .05 v/div
horz. 50 μsec.div

Fig. 6.5 Electroluminescence with pulse excitation. The upper trace is the applied voltage and the bottom trace is the elctro-luminescence brightness.

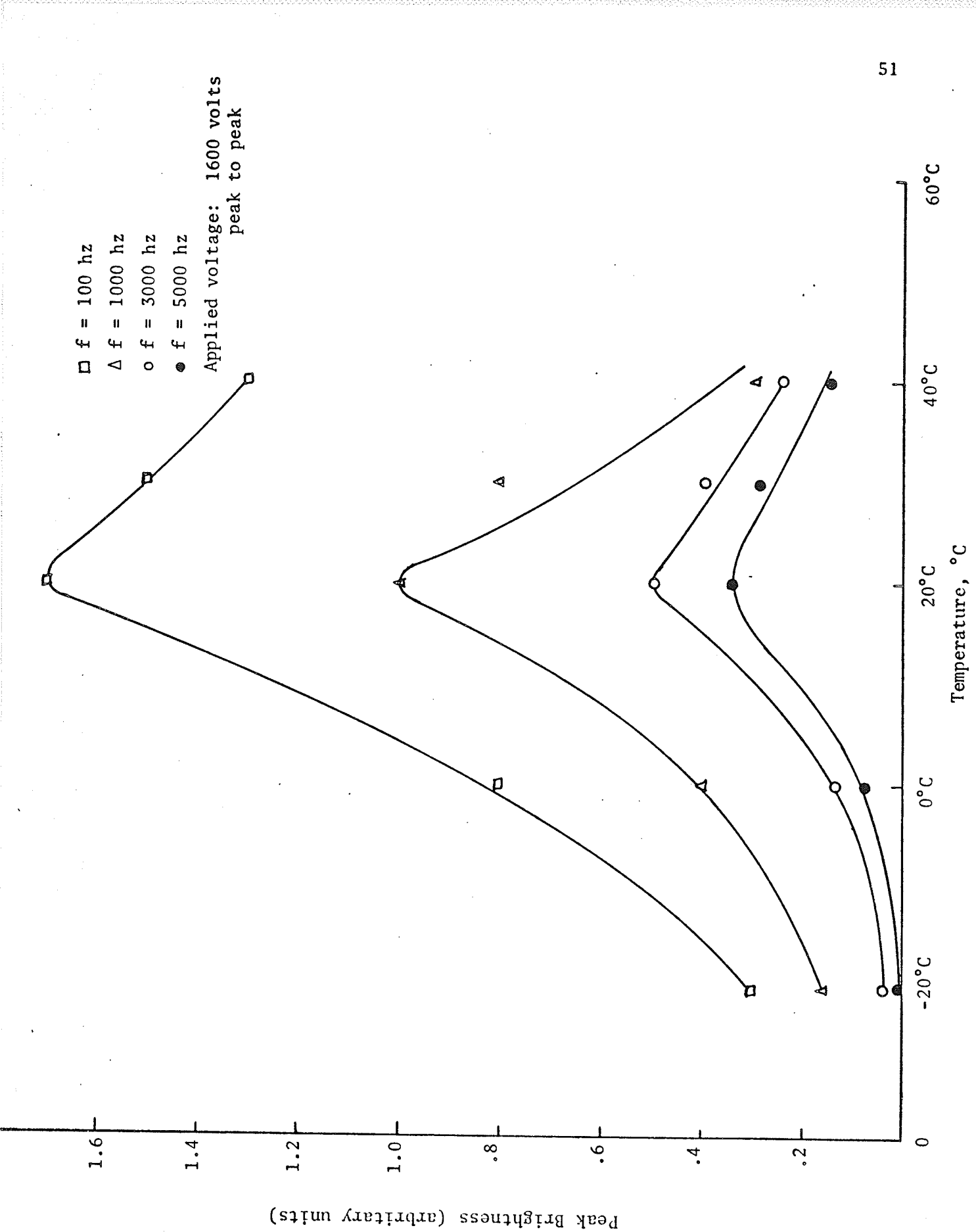

Fig. 6.6 Temperature dependence of a.c. electroluminescence

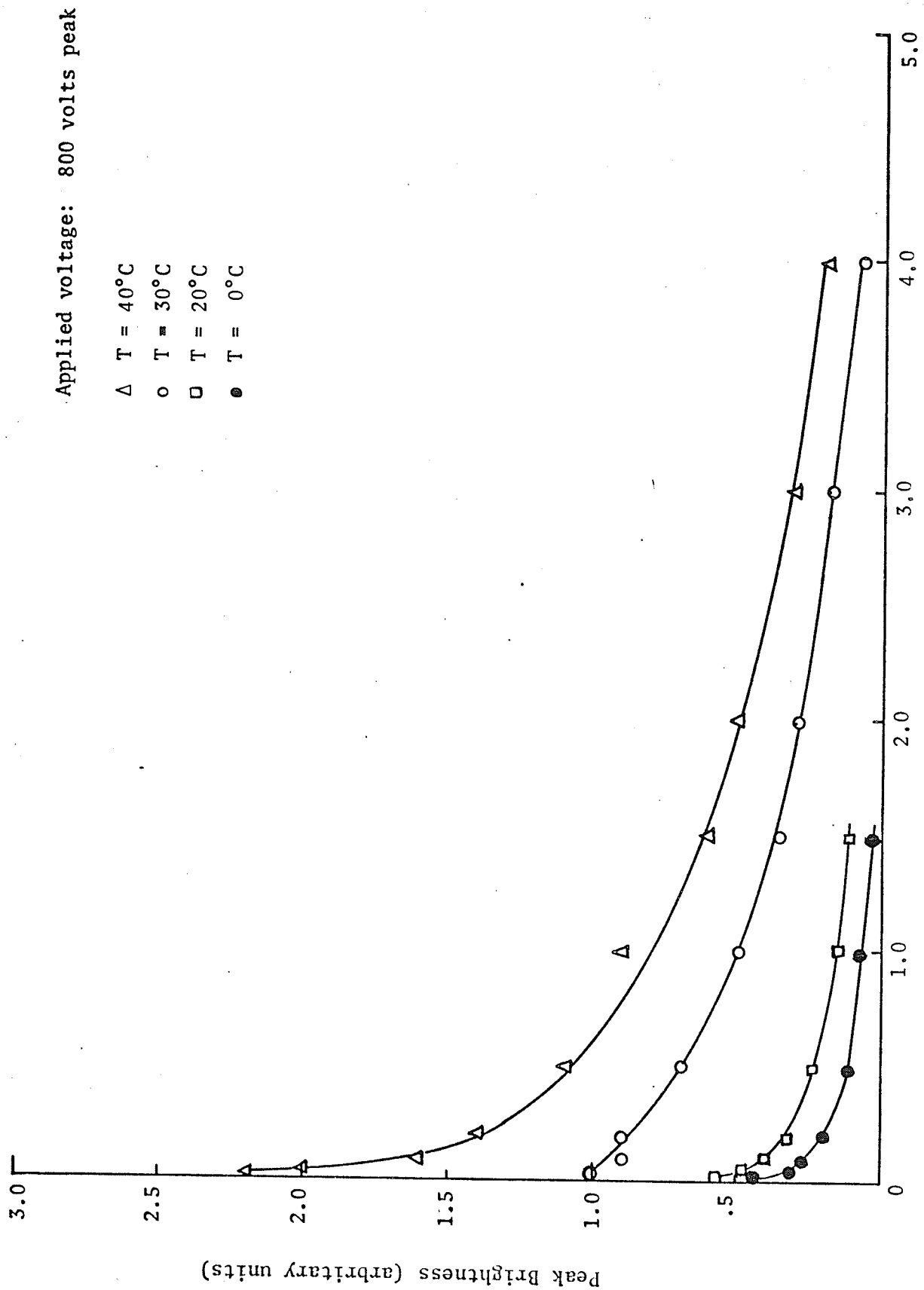

Fig. 6.7 Frequency dependence of brightness for a half-wave rectified voltage

brightness obtained if a d.c. voltage of 800 volts was applied.

6.2.2 Time Dependence of Electroluminescence

The series of photographs given in Figure 6.8 show that as in a.c. electroluminescence there is a delay time between the time when the voltage is applied and the time when the electroluminescence appears. The photographs were taken with the crystal temperature at approximately 40°C. The electroluminescence waveform has the same form as that of the voltage at low frequencies (20 Hz) but at high frequencies (> 2 kHz) a significant exponential tail developed on the trailing edge which stretches well into the time region in which the applied voltage is zero.

A frequency dependent phase shift again appears between the peak applied voltage and the peak electroluminescent brightness. The phase shift increases with increasing frequency. Figure 6.9 shows the frequency dependence of the turn-on and turn-off threshold voltage at 40°C. The upper cruve represents the voltage at which the electroluminescence first appears; and the lower curve, the voltage at which the elctroluminescence waveform develops an exponential tail. The curves indicated qualitatively how the phase shift varies with frequency. At low frequencies the turn-on and turn-off voltages are equal and the electroluminescence is in phase with the voltage. When the frequency is large (5 kHz) the electroluminescence does not even appear until the positive half-cycle of the voltage is near its maximum.

6.2.3 Temperature Dependence of Electroluminescence

Figure 6.10 shows the temperature dependence of the electroluminescent brightness for temperatures between 0°C and 40°C. The brightness increases with increasing temperature. It is expected that a peak in the temperature

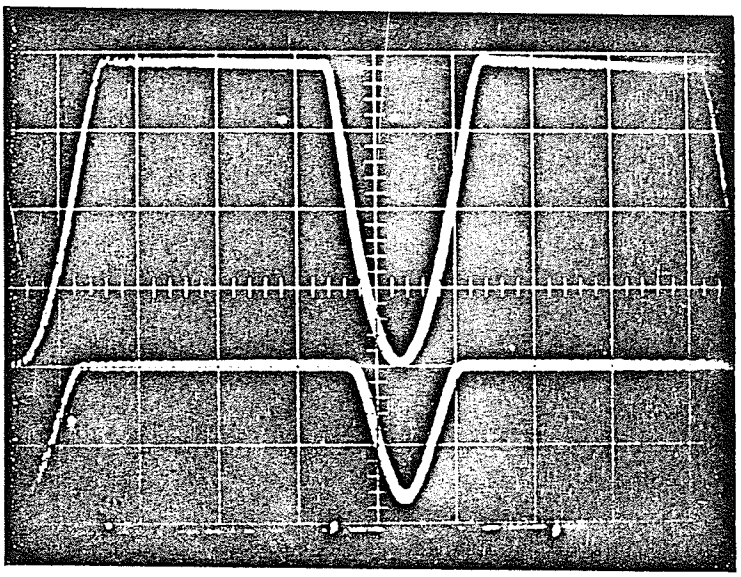

(a)

Scale: vert. voltage 200 v/div
brightness .1 v/div
horz. 10 msec/div

Frequency: 20 Hz

Fig. 6.8 Time dependence of electroluminescence under a half-wave rectified voltage at various repetition rates. The upper trace is the applied voltage and the bottom trace is the electroluminescence brightness.

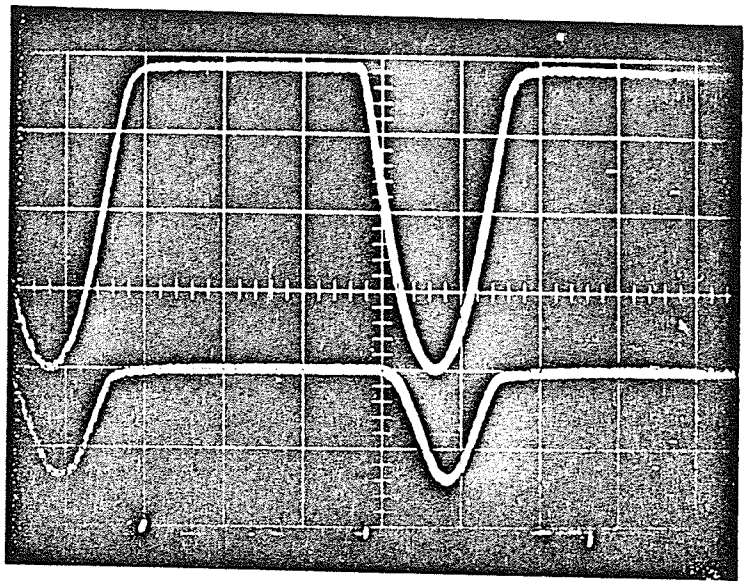

(b)

Scale: vert. voltage 200 v/div
brightness .1 v/div
horz. 1 msec/div

Repetition rate: 200 Hz

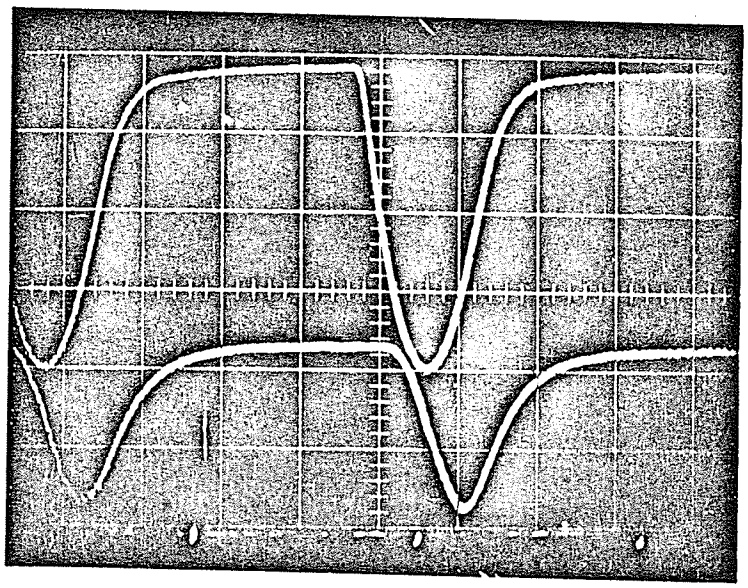

(c)

Scale: vert. voltage 200 v/div
brightness .02 v/div
horz. 50 μsec/div

Repetition rate: 2KHz

Fig. 6.8 Time dependence of electroluminescence under a half-wave rectified voltage at various repetition rates. The upper trace is the applied voltage and the bottom trace is the electroluminescence brightness.

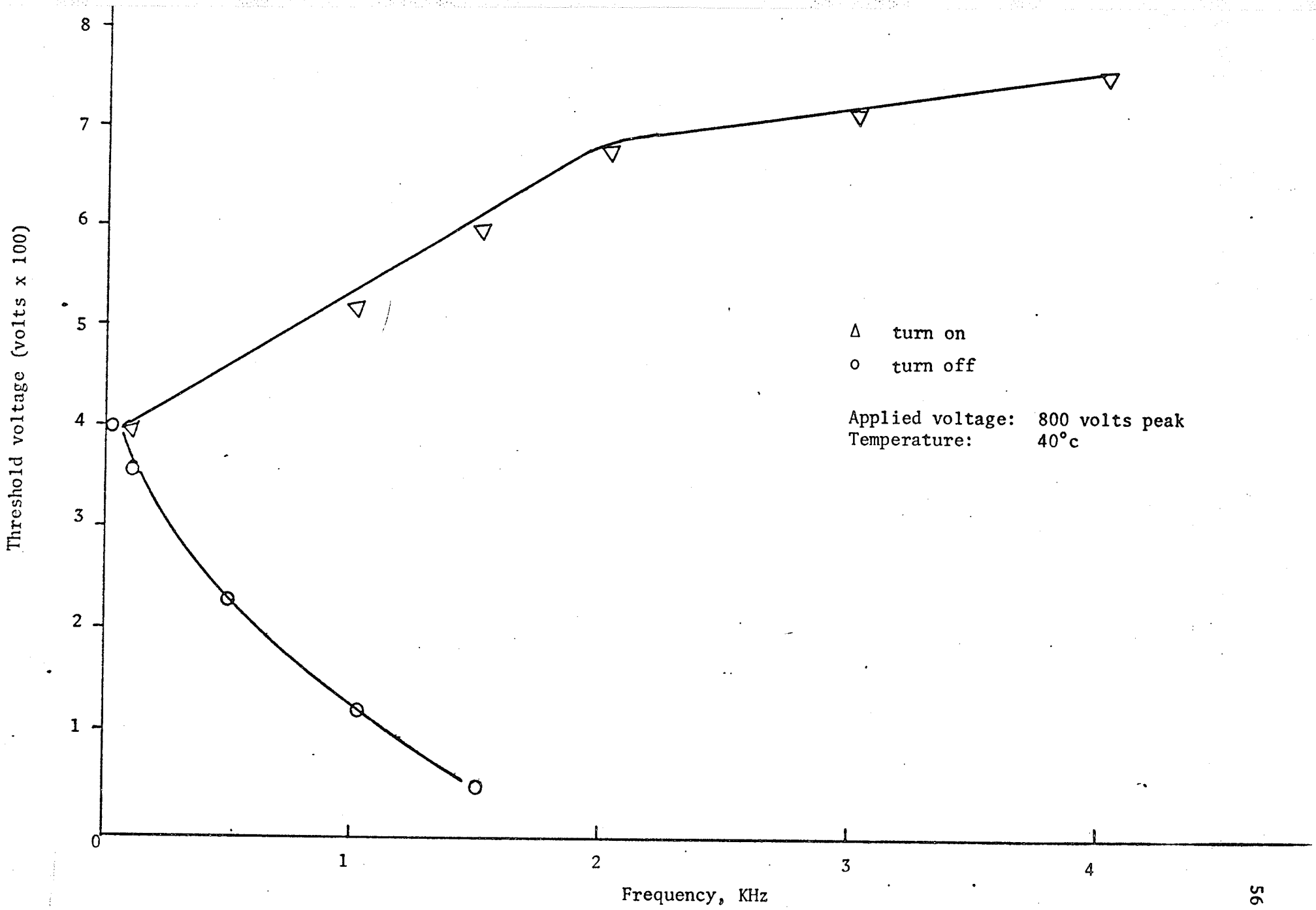

Fig. 6.9 Frequency dependence of the threshold voltage

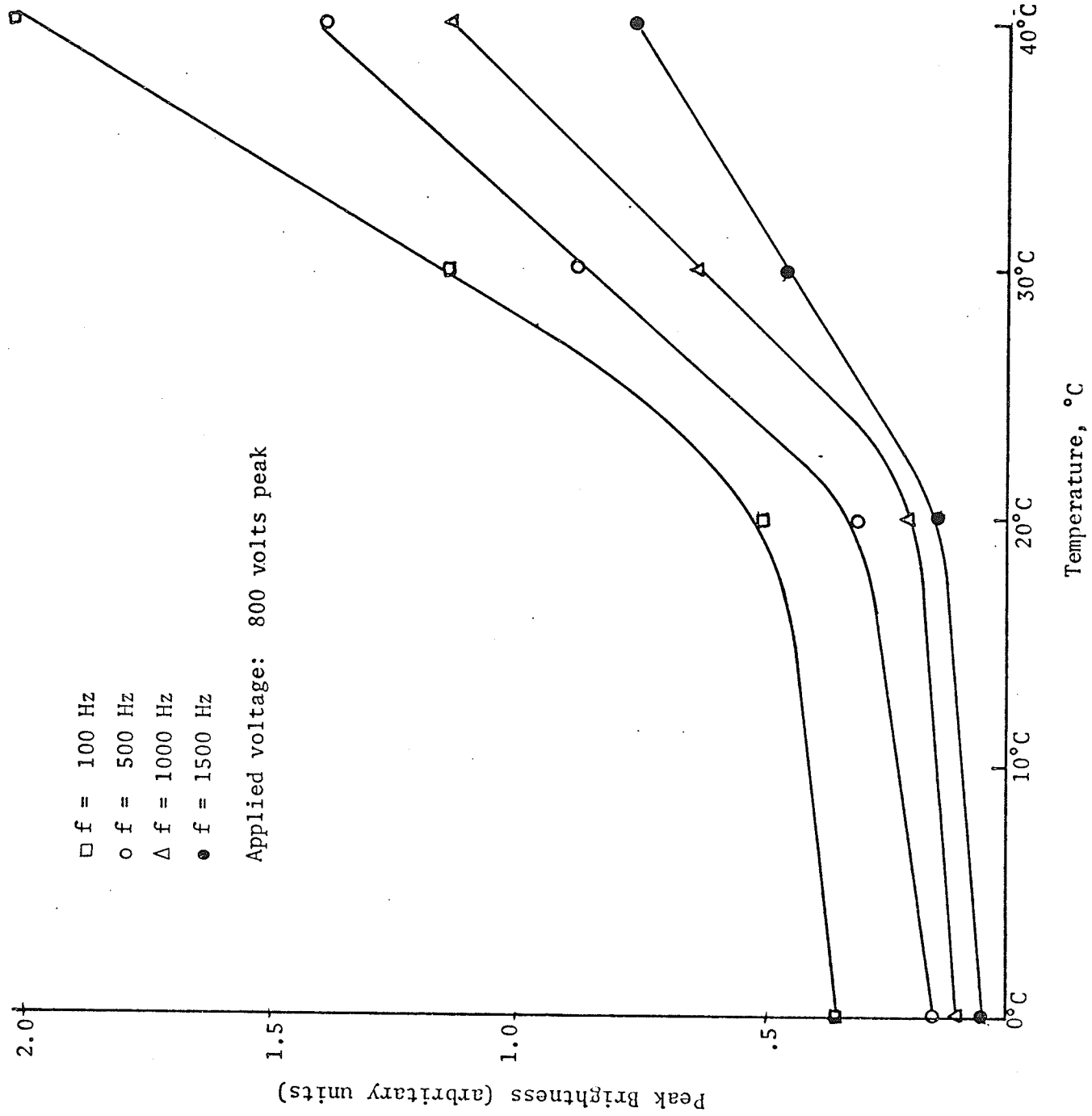

Fig. 6.10 Temperature dependence of electroluminescence produced with half-wave rectified voltage, at various frequencies

dependence exists above 40°C. Hwang and Kao [18] have found a peak in the d.c. electroluminescent brightness at approximately 40°C for a crystal obtained from the same source. It is expected that under a half-wave rectified voltage the electroluminescence may behave similarly because of the unidirectional nature of the field. Measurements could not be made above 40°C because the protective wax layer for the sodium electrode would soften and cause the sodium electrode to be oxidized. It is of interest to note that the peak in the temperature dependence of the brightness for a.c. voltages occurred at a lower temperature (Fig. 6.6.).

6.3 Discussion of Experimental Results

In anthracene the hole and electron mobilities are small and the carrier recombination rate constant is large [14, 48]. Under these conditions double injection from two ohmic contacts will produce two space charge limited currents meeting and annihilating each other somewhere in the bulk of the crystal, thus causing electroluminescence. If the recombination rate, K, is sufficiently large the recombination will occur in an infinitely thin volume of the crystal. If a voltage step is applied to the crystal the current transient would have the same shape as that for a single injection space charge limited current. Figure 6.11a shows the form of the current transient. The value of K, though large, is finite, however, and thus some space-charge overlap does occur. The width of the recombination zone is given by [48]

$$W = \frac{4e\,\mu_e\,\mu_h\,L}{K\,\varepsilon\varepsilon_o\,(\mu_e + \mu_h)} \qquad (6.1)$$

and the time required for the two space charge limited currents to meet each other after the voltage is applied is given by [14]

$$\tau_m = 0.79 \left[\frac{L^2}{(\mu_e + \mu_h)V} \right] \qquad (6.2)$$

where μ_e and μ_h are the mobilities of the electrons and holes respectively, L is the crystal thickness, ε the permittivity and V is the applied voltage. The dashed curve in Figure 6.11a shows how the current transient continues after τ_m, that is after the space-charge overlap develops. Figure 6.11b shows the light transient after some space charge overlap develops.

The d.c. electroluminescent brightness has been found to be independent of the nature of the hole injecting contact if the electron injecting electrode can supply a large electron current [48]. For a pulsed excitation, however, the current transit time with double injecting electrodes indicates an effective mobility equal to $\mu_e + \mu_h$. If the hole injecting contact is normally a blocking contact (such as silver) the transit time indicates an effective carrier mobility equal to the electron mobility only [48, 14, 30]. In the latter case the electroluminescence would appear only when the electon space charge front arrives at the anode. We have found that the rise of the slow electroluminescence after the application of a step voltage is not related to the triplet lifetime for our electrode combination. The variation with time of the electroluminescent brightness depended on the current and could last several minutes.

To account for the enhanced hole injection from normally blocking contacts and the time dependence of the injection Williams and Schadt [48] have suggested thatthe arriving electron space charge at the anode would modify the Schottky barrier and thus increase the "transparency" of the barrier to holes [14]. It is expected that the presence of impurities in the sample would have an effect on the injection mechanism by trapping the injected carriers and limiting the degree of barrier modification.

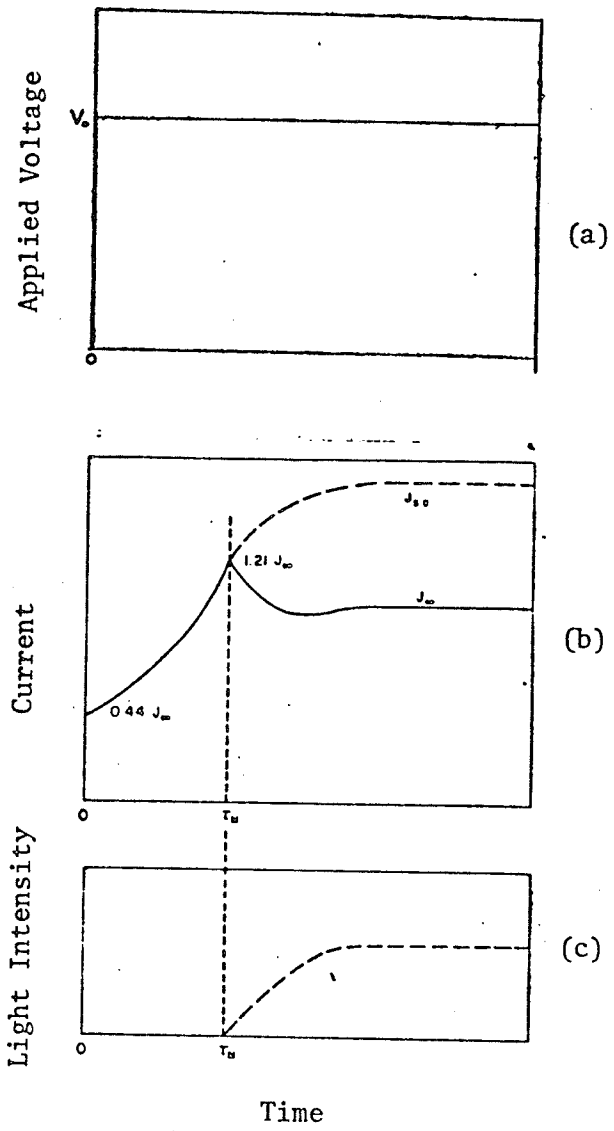

Fig. 6.11 Current and light transients produced upon application of a step voltage
(a) step voltage
(b) current transient after application of a step voltage
(c) electroluminescence transient after the occurence of overlap of the two injected currents.

The electroluminescence rise time would thus depend not only on the voltage but also on the crystal purity.

For low injection for which the space charge effect can be ignored, the transit time of the carrier can be expressed as

$$\tau_o = \frac{L^2}{\mu V} \tag{6.3}$$

If a large charge reservoir exists at the cathode (perfect ohmic contact) the space charge limited transient is similar to that shown in Figure 6.11a. Because of the existence of the space charge the transit time, τ_r, is reduced to [23]

$$\tau_r \simeq 0.786\ \tau_o \tag{6.4}$$

where τ_o is space charge free transit time. The above two cases are the two extremes and the acutal transit time could lie somewhere between the two.

The above argument is based on a step excitation. If the excitation is removed after a time equal to or greater than the transit time the transient prior to this will be unaffected.

6.3.1 Frequency Dependence of Electroluminescence

Because of the finite transit time of the electrons across the sample no light output will be observed unless one-half the period of the voltage is greater than the transit time.

$$\frac{T}{2} \geq \tau_r \tag{6.5}$$

where T is the period of the applied voltage. The frequency at which the electroluminescence disappear is thus given by

$$f_\ell \simeq \frac{1}{2\tau_r} \tag{6.6}$$

This result would be applicable only for the sinusoidal excitation since after each positive half cycle all excess carriers in the sample that have not recombined must be driven out of the crystal by the negative half cycle. If the mobility of the electrons is assumed to be independent of the field and the time taken for the electron space charge to build up and modify the barrier at the hole injecting contact is assumed to be small compared to the transit time, then we can use the value obtained from Figure 6.5 for the high frequency delay time (30 μsec) as an approximate value of the electron transit time. Thus the upper limit for a.c. electroluminescence is given by

$$f_\ell \simeq 12 \text{ kHz}$$

for the sample of thickness .4 mm used for the present investigation. This agrees fairly well with the experimental results obtained. Electroluminescence was still detectable at frequencies as high as 10 kHz, although the signal was very small. In the case of a half-wave rectified a.c. excitation the crystal is not completly emptied of excess carriers after the elapse of each positive half cycle, and consequently the upper limit on the frequency is higher than f_ℓ. In both cases, however, as the frequency increases the number of electrons that can be injected and transported to the anode decreases. Thus the electroluminescence output per cycle as well as the peak electroluminescent brightness decreases with frequency. The integrated light output has also been found to decrease with increasing frequency. Since the integrated light output would depend on both light output per cycle and the repetition rate, we can conclude that the light ouput per cycle decreases at a rate greater than $\frac{1}{f}$. The brightness of the electro-

luminescence for the rectified a.c. excitation is expected to be larger than the a.c. electroluminescence at any given frequency because of the excess charge that remains in the crystal during the off time. Thus more electrons will reach the anode during the positive half-cycle.

The exponential tail observed in the electroluminescence waveform may be caused by the delayed flourescence generated by triplet-triplet annihilations. The lifetime of the triplet exciton is of the order of milli seconds [48] and thus after the excitation ceases the flourescence does not cease immediately. It decays with a time constant related to the triplet lifetime. Thus the exponential tail exists on the electroluminescence waveform at all frequencies but becomes much more pronounced at higher frequencies.

The fact that electroluminescence appeared only on the half cycle in which the silver electrode was positive and the sodium electrode was negative indicates that the sodium electrode is an excellent electron injecting contact and consequently a very poor hole injector.

6.3.2 Time Dependence of Electroluminescence

The delay between the time at which the voltage is applied and the time at which the electroluminescence appears depends on both the electron transit time and the time taken to modify the barrier at the anode. Since the modification of the barrier depends on the presence of electron space charge in the vicinity, the time taken to modify the barrier should be proportional to the voltage. Hwang and Kao [18] have found that the threshold voltage for d.c. electroluminescence is affected by the on-and-off time. If the excitation is removed and immediately switched on again the threshold voltage is reduced. If the switch-off time is increased then

the threshold voltage would approach the initial value again. This suggests that the relaxation of the barrier at the minority carrier injecting contact takes a finite time which may be associated with the time it takes for the excess space charge to relax. A similar effect is noticed in electroluminescence with time-varying fields. As the repetition rate increases the barrier for hole injection does not completely relax. It takes less injected charge to induce the hole injection during each cycle. Figure 6.4 shows the frequency dependence of the delay time for a.c. electroluminescence. As the frequency increases the delay time decreases rapidly and saturates at a value which is probably equal to the electron transit time. The delay time is comparable to the actual transit time measured when a 800 volt rectangular pulse is applied. (Figure 6.5b)

It should be noted that the transit time at high frequencies may be considered to be approximately equal to the space-charge-free transit time τ_o. In the case of low frequencies the space-charge-limited transit time may be more accurate. Thus even for two ohmic contacts one would expect a frequency-dependent delay time. Since the excitation is not a step excitation both delay times can be expected to be somewhat larger. Replacing the applied voltage by an average value we have that, in the high frequency range

$$\tau_o = \frac{L^2}{\mu \bar{V}} \tag{6.7}$$

We can roughly estimate the electron mobility by assuming that the recombination occurs near the anode. At 20°C the delay time at high frequencies (5 kHz) was 25 μsec. The sample thickness was .4 mm. This yield a mobility of 0.16 cm^2/v-sec. This roughly agrees with the accepted value

of .4 cm^2/v-sec. The mobility of the electrons can also be estimated from the frequency dependence of the electroluminescent brightness. It is assumed that the recombination zone is at the anode and the electroluminescence disappears when the half cycle time is equal to the transit time. Therefore, we have

$$\tau_o = \frac{T}{2} = \frac{1}{2f_\ell} = \frac{L^2}{\mu V} \tag{6.8}$$

The frequency at which the electroluminescence was no longer detectable was 10 kHz. This gives an electron mobility of .08 cm^2/v-sec.

The apparent phase shift between the electroluminescence and the applied voltage cannot be separated from the delay time. The phase shift is a result of the finite delay time between the peak electroluminescent brightness and the voltage, which becomes comparable to the period at high frequencies. For instance at 5 kHz the delay time is 30 μsec and the half cycle time is 100 μsec.

6.3.3 Temperature Dependence of Electroluminescence

The temperature dependence of electroluminescence under a half wave rectified voltage showed an increasing brightness with increasing temperature in the temperature range 0°C to 40°C. It was indicated that a peak was expected at a temperature larger than 40°C. The temperature dependence of a.c. electroluminescence, however, has a peak at 20°C. The temperature dependence of d.c. electroluminescence has been explained in terms of exciton carrier interactions and the detrapping of trapped carriers [19]. It is expected that the peaks observed for electroluminescence under time varying fields are also caused by these two processes. The fact that the result for the a.c. electroluminescence has a peak at 20°C while the rectified a.c. electroluminescence increases up to 40°C is believed

to be due to the larger space charge supplied to the crystal by the rectified a.c. voltage. It is expected that the change in temperature will affect the trapped carrier concentration much more than the carrier injection from the electrodes. This increase in free carrier density causes the increase in brightness at low temperatures. The larger space charge resulting from the rectified a.c. voltage will dominate the free carriers produced by the detrapping processes at higher temperatures, than the space charge produced by the a.c. voltage. The peak in the brightness-temperature curve is thus shifted to higher temperatures for the case of the rectified a.c. voltage. At these temperatures the free carriers produced by detrapping become comparable in concentration to the injected carriers. At higher temperatures the brightness decreases with temperature because the interaction of excitons with carriers becomes the dominant process.

The probability of detrapping a carrier is given by

$$P = \nu \exp \left[- \frac{E_t}{kT} \right] \tag{6.9}$$

where ν is the carrier-attempt-escape frequency and E_t is the depth of the carrier trap. The rate of exciton carrier interactions is given by

$$K = ZN_T \tag{6.10}$$

where N_T is the total carrier density and Z is the rate constant for exciton-carrier interactions. The peak in the electroluminescence-temperature curve will occur when

$$\nu \exp \left[- \frac{E_t}{kT} \right] = ZN_T \tag{6.11}$$

Thus the peak occurs at a temperature given by

$$T_p = \frac{E_t}{\text{en } [\frac{\nu}{ZN_t}]} \tag{6.12}$$

It can be seen that with increasing carrier density the temperature T_p increases.

CHAPTER VII

CONCLUSIONS

On the basis of the present investigation, we can now draw the following conclusions.

(1) The electroluminescence brightness decreases monotonically with increasing frequency for both a.c. and rectified a.c. voltages.

(2) For the electrodes used (sodium and silver) electroluminescence was observed only when the sodium was negative and the silver was positive in potential.

(3) The temperature dependence of the electroluminescent brightness has a peak at 20°C for an applied a.c. voltage and the brightness decreases on either side of this critical temperature. For the case of the half-wave rectified voltage the brightness increased with increasing temperature in the temperature range 0°C to 40°C and is expected to have a peak at a temperature above 40°C.

(4) There is a time delay between when the positive half cycle of the voltage begins and when the electroluminescence appears. The time delay decreases with increasing frequency.

(5) The electroluminescence has the same shape as the applied voltage for low frequencies (20 Hz). For high frequencies a significant exponential tail is observed on the trailing edge (frequencies larger than 2 KHz).

(6) From the results the electron mobility has been estimated to be approximately .16 cm^2/v-sec as compared to an accepted value of .4 cm^2/v-sec. The lower value predicted may be due to the assumption that the time for the build up of space charge to modify the hole-injecting barrier is negligible compared to the electron transit time.

(7) Electroluminescence does not appear until the electron space charge front arrives at the anode. The electron space charge modifies the barrier at the anode and produces enhanced hole injection.

REFERENCES

[1] Adolf, J. and Williams, D.F., "Temperature dependence of singlet-triplet intersystem crossing in anthracene crystals", J. Chem. Phys. 46, 4248-51 (1967).

[2] Arnold, S., Witten, W.B. and Damask, A.D., "Triplet exciton trapping by dislocations in anthracene", J. Chem. Phys. 53, 2878-2884 (1970).

[3] Avakian, P., Ern, V., Merrifield, R.E. and Suna, A., "Spectroscopic approach to triplet exciton dynamics in anthrance", Phys. Rev. 165, 974-80 (1968).

[4] Avakian, P. and Merrifield, R.E., "Triplet excitons in anthracene crystals - a review", Mol. Cryst. 5, 37-77 (1968).

[5] Baesaler, H. and Vaubel, G., "Surface states of anthracene crystals", Phys. Rev. Lett. 21, 615-17 (1968).

[6] Barnett, A.M., "Current Filament Formation", in Semi-conductors and Semi-Metals, Williamson, R.K. and Beer, A.C. Eds., Academic Press, New York, Vol. 6, 141-200 (1970).

[7] Caywood, J.M., "Photoemission from metal contacts into anthracene crystals: A critical review", Mol. Cryst. Liquid Cryst. 12, 1-26, (1970).

[8] Dexter, D.L. and Knox, R.S., Excitons, Interscience Publishers, New York, (1965).

[9] Ern, V., Avakian, P. and Merrifield, R.F., "Diffusion of triplet excitons in anthracene crystals", Phys. Rev. 148, 862-67 (1966).

[10] Ern, V., Bouchriha, H., Fourny, J. and Delacote, G., "Triplet exciton-trapped hole interaction in anthracene crystals", Solid State Commun. 9, 1201-1203 (1971).

[11] Goode, D.H. and Lipsett, F.R., "Delayed flourescence of anthracene at low temperature. Failure of square dependence of exciting light", J. Chem. Phys. 51, 1222-28 (1969).

[12] Helfrich, W. and Schneider, W.G., "Recombination radiation in anthracene crystals", Phys. Rev. Lett. 14, 229-231 (1965).

[13] Helfrich, W., "Destruction of triplet excitons in anthracene by injected electrons", Phys. Rev. Lett. 16, 401-403 (1966).

[14] Helfrich, W. and Schneider, W.G., "Transients of volume-controlled current and of recombination radiation in anthracene", J. Chem. Phys. 44, 2902-2909 (1966).

[15] Hoesterey, D.C. and Robinson, G.W., "On the diffusion coefficient of triplet excitons in anthracene", J. Chem. Phys. 54, 1709-12 (1970).

[16] Hwang, W. and Kao, K.C., "A unified approach to the theory of current injection in solids with traps uniformly and non-uniformly distributed in space and energy, and size effects in anthracene films", Solid State Electron. 15, 523-9 (1972).

[17] Hwang, W. and Kao, K.C., "A unified approach to the theory of double injection in solids with traps uniformly and non-uniformly distributed in the energy band gap", Solid State Electron. 16, 407-415 (1973).

[18] Hwang, W. and Kao, K.C., "Electroluminescence in anthrance crystals caused by field induced minority carriers at moderate temperatures", J. Chem. Phys. 58, 3521-22 (1973).

[19] Hwang, W. and Kao, K.C., "On the theory of filamintory double injection and electroluminescence in molecular crystals", J. Chem. Phys. 60, 3845-55 (1974).

[20] Kepler, R.G., Caris, J.C., Avakian, P. and Abramson, E., "Triplet excitons and delayed flourescence in anthracene crystals", Phys. Rev. Lett. 10, 400-402 (1963).

[21] Kepler, R.G. and Switendick, A.C., "Diffusion of triplet excitons in anthracene", Phys. Rev. Lett. 15, 56-59 (1965).

[22] Knox, R.S., Theory of Excitons, Academic Press, New York, (1963).

[23] Lampert, M.A. and Mark, P. Current Injection in Solids, Academic Press, New York, (1970).

[24] McMahon, D.H. and Kestigram, M., "Triplet-triplet annihilation in anthracene at low excitation intensities-wavelength and temperature dependence", J. Chem. Phys. 46, 137-142 (1967).

[25] Mehl, W. and Funk, B., "Dark injection of electrons and holes and radiative recombination in anthracene with metallic contacts", Phys. Lett. 25A, 364-365 (1967).

[26] Morris, R. and Silver, M., "Direct electron-hole recombination in anthracene", J. Chem. Phys. 50, 2669-2973 (1969).

[27] Paramenter, R.H. and Ruppel, W., "Two-carrier space-charge limited current in a trap-free insulator", J. Appl. Phys. 30, 1548-1558 (1959).

[28] Paul, D.E., Lipkin, D and Weissman, S.I. "Reactions of sodium metal with aromatic hydrocarbons", J. Chem. Phys. 78, (1955).

[29] Pope, M., Kallmann, H.P. and Magnante, P., "Electroluminescence in organic crystals", J. Chem. Phys. 35, 2042-2043 (1963).

[30] Pott, G.T. and Williams, D.F., "Low temperature electron injection and space-charge limited transients in anthracene crystals", J. Chem. Phys. 51, 1901-1906 (1969).

[31] Sano, M., Pope, M. and Kallmann, H., "Electroluminescence and band gap in anthracene", J. Chem. Phys. 43, 2920-2921 (1965).

[32] Schadt, M. and Williams, D.F., "Low temperature hole injection and hole trap distribution in anthracene", J. Chem. Phys. 50, 4364-68 (1969).

[33] Schwob, H.P., Funfschilling, J. and Zschokke-Granacher, I., "Recombination radiation and flourescence in doped anthracene crystals", Mol. Cryst. and Liquid Cryst. 10, 39-45 (1970).

[34] Schwob, H.P. and Zschokke-Granacher, I., "Doppelinjection and elektrolumineszenz in dotierton anthracenkristallen", Mol. Cryst. and Liquid Cryst. 13, 115-136 (1971).

[35] Siebrand, W., "Trapping of triplet excitons and the temperature dependence of delayed flourescence in anthracene crystals", J. Chem. Phys. 42, 3951-54 (1965).

[36] Singh, S., Jones, W.J., Siebrand, W. Stoicheff, B.P. and Schneider, W.G., "Laser generation of excitons and flourescence in anthracene", J. Chem. Phys. 42, 330-342 (1965).

[37] Singh, S. and Lipsett, F.R., "Effect of purity and temperature on the flourescence of anthracene excited by red light", J. Chem. Phys. 41, 1163-64 (1964).

[38] Silver, M and Sharma, R. "Carrier generation and recombination in anthracene", J. Chem. Phys. 46, 692-696 (1967).

[39] Smith, G.C., "Triplet exciton phosphorescence in crystalline anthracene", Phys. Rev. 166, 839-847 (1968).

[40] Suna, A., "Kinematics of exciton-exciton annihilation in molecular crystals", Phys. Rev. B1, 1716-1739 (1970).

[41] Uityuk, N.V. and Mikho, V.V., "Electroluminescence of anthracene excited by π-shaped voltage pulses", Soviet Phys. - Semicon 6, 1497-1499, (1973).

[42] Wakayama, N. and Williams, D.F., :Singlet exciton-charge carrier interactions in anthracene", Chem. Phys. Lett. 9, 45-47 (1971).

[43] Wakayama, N. and Williams, D.F., "Carrier-exciton interactions in crystalline anthracene", J. Chem. Phys. 57, 1770-1779 (1972).

[44] Williams, D.F. and Schneider, W.G., "Phosphorescence emission from anthracene single crystals", J. Chem. Phys. 45, 4756-4757 (1966).

[45] Williams, D.F., Adolph, J. and Schneider, W.A., "Diffusion of triplet exciton in anthracene crystals", J. Chem. Phys. 45, 575-577 (1966).

[46] Williams, D.F. and Adolph, J., "Diffusion length of triplet excitons in anthracene crystals", J. Chem. Phys. 46, 4252-4254 (1967).

[47] Williams, D.F. and Schadt, M., "A simple organic electroluminescent diode", Proc. IEEE 58, 476 (1970).

[48] Williams, D.F. and Schadt, M., "DC and pulsed electroluminescence in anthracene and doped anthracene crystals", J. Chem. Phys. 53, 3480-3487 (1970).

[49] Williams, R. and Dresner, J., "Photoemission of holes from metals into anthracene", J. Chem. Phys. 46, 2133-2138 (1966).

[50] Williams, W.G. and Spong, P.L. and Gibbons, D.J., "Double injection electroluminescence in anthracene and carrier injection properties of carbon fibres", J. Phys. Chem. Solids 33, 1879-1884 (1972).